Investigation of the Evolution of Conduction Mechanism

In Metal on Transparent Conductive Oxides

Thin Film System

by

Shengke Zhang

A Thesis Presented in Partial Fulfillment
of the Requirements for the Degree
Master of Science

Approved April 2012 by the
Graduate Supervisory Committee:

Terry Alford, Chair
Amaneh Tasooji
Dieter Schroder

ARIZONA STATE UNIVERSITY

May 2012

ABSTRACT

This thesis discusses the evolution of conduction mechanism in the silver (Ag) on zinc oxide (ZnO) thin film system with respect to the Ag morphology. As a plausible substitute for indium tin oxide (ITO), TCO/Metal/TCO (TMT) structure has received a lot of attentions as a prospective ITO substitute due to its low resistivity and desirable transmittance. However, the detailed conduction mechanism is not fully understood. In an attempt to investigate the conduction mechanism of the ZnO/Ag/ZnO thin film system with respect to the Ag microstructure, the top ZnO layer is removed, which offers a better view of Ag morphology by using scanning electron microscopy (SEM). With 2 nm thick Ag layer, it is seen that the Ag forms discrete islands with small islands size (r), but large separation (s); also the effective resistivity of the system is extremely high. This regime is designated as dielectric zone. In this regime, thermionic emission and activated tunneling conduction mechanisms are considered. Based on simulations, when “s” was beyond 6 nm, thermionic emission dominates; with “s” less than 6 nm, activated tunneling is the dominating mechanism. As the Ag thickness increases, the individual islands coalesce and Ag clusters are formed. At certain Ag thickness, there are one or several Ag clusters that percolate the ZnO film, and the effective resistivity of the system exhibits a tremendous drop simultaneously, because the conducting electrons do not need to overcome huge ZnO barrier to transport. This is recognized as percolation zone. As the Ag thickness grows, Ag film becomes more continuous and there are no individual islands left on the surface. The effective resistivity decreases and is comparable to

the characteristics of metallic materials, so this regime is categorized as metallic zone. The simulation of the Ag thin film resistivity is performed in terms of Ag thickness, and the experimental data fits the simulation well, which supports the proposed models. Hall measurement and four point probe measurement are carried out to characterize the electrical properties of the thin film system.

DEDICATION

To my parents Bin Zhang and Yongpin Zhang, who have loved and supported me through all my life, my grandparents who cared for me, and my girlfriend Fei Gao who makes everything worth it.

ACKNOWLEDGMENTS

I am greatly indebted to Dr. Terry Alford for giving me an opportunity to work in this great group and give me a lot of insightful advice. I cannot appreciate enough Rajitha Vemuri, Hyung Choi, Aritra Dhar, and Sanyantan Das for all the insights and support that they offered.

I would like to express my appreciation to Prof. Dieter Schroder, Prof. Amaneh Tasooji, and Dr. David Theodore for being my committee, and taking time to evaluate my thesis work.

I thank all my friends who have always supported me, encouraged me, and positively criticized me.

This project is partially supported national science foundation (L. Hess, Grant No. DMR-0602716) to whom the authors are greatly indebted.

TABLE OF CONTENTS

PAGE

LIST OF TABLES.....viii

LIST OF FIGURES.....ix

CHAPTER

1 INTRODUCTION.....1

1.1 Thin Film Growth.....1

1.2 Transperant Conductive Oxides (TCOs).....2

1.2.a Popular TCOs.....2

1.2.b Doping TCOs.....3

1.2.c TCO/Metal/TCO (TMT) Structure.....3

1.3 Thin Film Conduction Mechanism …….....5

1.3.a Thermionic Emission.....5

1.3.b Tunneling.....6

1.4 Electron Mean Free Path.....7

2 EXPERIMENTAL PROCEDURE.....8

2.1 Sample Preparation.....8

2.1.a Diode Sputtering.....8

2.1.b Radio Frequency Sputtering.....9

2.2 Materials Characterization.....10

2.2.a Rutherford Backscattering Spectrometry.....10

2.2.b Scanning Electron Microscopy.....12

2.2.c Hall Measurement.....15

CHAPTER PAGE

2.2.d Four Point Probe Measurement.....20

3 SIMULATION OF EVOLUTION OF CONDUCTION MECHANISM IN THIN SILVER ON ZINC OXIDE.....23

3.1 Introduction.....23

3.2 Literature Background.....24

3.2.a Dielectric Zone.....25

3.2.b Thermionic Emission.....27

3.2.c Tunneling.....31

3.2.d Percolation Theory.....38

3.2.e Metallic Zone.....40

3.3 Simulation Procedure.....44

3.4 Simulation Results.....45

3.4.a Simulation of Conduction Mechanism in the Dielectric Zone.....46

3.4.b Simulation of Resistivity in Metallic Zone.....49

3.5 Discussion.....50

3.6 Conclusion.....53

4 THE EFFECT OF SILVER THICKNESS ON THE ELECTRICAL AND OPTICAL PROPERTIES OF Ag/ZnO WITH RESPECT TO THE Ag MIRCOSTRCTURE.....54

4.1 Introduction.....54

4.2 Experimental.....55

CHAPTER PAGE

4.3 Results.....57

4.4 Discussion.....66

4.5 Conclusion.....71

5 Conclusions.....72

5.1 Summary.....72

5.2 Future Work.....73

REFERENCES 74

LIST OF TABLES

TABLE PAGE

1 The average islands size (r), inter-islands spacing, and Ag coverage at 2/4/6/8/10 nm Ag/ZnO thin film system.....61

2 The resistivity and sheet resistance of the 4/6/8/10 nm Ag/ZnO thin films on PEN substrate.....64

3 The resistivity and sheet resistance of 4/6/8/10 nm Ag/ZnO thin films on glass substrate.....64

LIST OF FIGURES

FIGURE PAGE

2.1. Schematic of a typical DC sputtering instrumentation system.....9

2.2. Schematic of a typical RF sputtering instrumentation system.....10

2.3. Schematic of a Rutherford backscattering spectrometry instrumentation system.....11

2.4. Schematic of a scanning electron microscopy instrumentation system.....13

2.5. Different types of scattered electrons after the primary electron beam interacted with the sample in the SEM.....14

2.6. Philips XL 30 scanning electron microscopy used at ASU.....15

2.7. Hall measurement sample labeled for the contacts.....16

2.8. Function mechanism of Hall measurement system.....19

2.9. Ecopia HMS-3000 Hall measurement system used at ASU.....20

2.10. Layout of a typical four point probe setup. Measurements taken at ASU had a probe spacing of 2 mm. Where s=spacing between the probes and t=the thickness of the sample.....21

2.11. Schematic of various types of resistance at the tip of the probe.....22

3.1. The top view of three stages of electrical characteristics of Ag/ZnO thin film system with respect to the evolution of Ag morphology..25

3.2. The side view of three stages of electrical characteristics of Ag/ZnO thin film system with respect to the evolution of Ag morphology..25

FIGURE PAGE

3.3. The Energy band diagram of Ag/ZnO/Ag structure before brought into contact and the vacuum energy levels line up.....27

3.4. The energy band diagram of Ag/ZnO/Ag structure after brought into contact and the Fermi levels line up.....28

3.5. The effective ZnO barrier height without considering the applied voltage (black), only considering the applied voltage (blue), and considering both applied voltage and image force effect (red).....29

3.6. The electrons near the Fermi level in left side Ag tunnel through the ZnO barrier and reach the new Fermi level in the right side Ag based on the quantum mechanical tunneling theory.....32

3.7. The electrons at the energy level δE above the original Fermi level in the left side Ag tunnel through the ZnO barrier and reach the Fermi level in the right side Ag based on the activated tunneling theory..36

3.8. Different color dots indicate the Ag islands sputtered on ZnO and they are grouped into certain clusters, and the blue cluster represents the percolating cluster.....39

3.9. The simulation of activated tunneling current density vs. the separation between two neighboring Ag islands.....46

3.10. The simulation of thermionic emission current density vs. separation between two neighboring Ag islands.....47

FIGURE PAGE

3.11. The overlay of Fig. 3.9 and 3.10, the activated tunneling is colored with blue, and the thermionic emission is in red. The total trend is marked as grey line.....48

3.12. The resistivity of thermionic emission and activated tunneling vs. the separation between two neighboring Ag islands.....49

3.13. The simulation of resistivity of Ag thin film vs. the thickness of the Ag film when p'=0, 0.5, and 1.....50

3.14. The simplified evolution of Ag morphology on the ZnO film in the dielectric zone.....51

3.15. The resistance series of Ag/ZnO film in the dielectric zone.....52

4.1. SEM images from (a) to (j) show the evolution of Ag microstructure with respect to the Ag thickness of 2/4/6/8/10 nm on PEN and glass substrate.....58

4.2. (a) to (j) show the evolution of r and s with respect to the Ag thickness of 2/4/6/8/10 nm on glass substrate.....60

4.3. The evolution of the average islands size with respect to the Ag thickness varying from 2nm to 10nm.....62

4.4. The evolution of the average inter-islands spacing with respect to the Ag thickness varying from 2nm to 10nm.....62

4.5. The evolution of the Ag coverage with respect to the Ag thickness varying from 2nm to 10nm.....62

4.6. The resistivity vs. Ag thickness on PEN and glass substrate.....64

FIGURE PAGE

4.7. The sheet resistance vs. Ag thickness on PEN and glass substrate.....65

4.8. The Ag thin film morphology and series resistance model in the dielectric zone.....67

4.9. The percolating clusters were marked in the 4nm Ag/ZnO thin film system.....68

4.10. The parallel resistance of Ag/ZnO thin film system when the Ag thickness was beyond the percolation threshold.....70

Chapter 1

INTRODUCTION

1.1. Thin Films Growth

Due to the growing demands for more portable and convenient electronic devices, the size of electronic devices has shrunk tremendously in recent decades, but the increasing desires for faster processing speed and multi-functions devices contrarily require more volume and space, which is the driving force for new smaller-scale technologies. Thin film, a technology coined by depositing materials on the substrate in the nanometer-scale thick, becomes a very popular topic and offers a new perspective in both research and industrial fields. However, as the thickness of materials scales down to nanometer-scale, the physical properties become different, sometimes even significantly different from the corresponding bulk ones. Therefore, in order to process thin film materials with desirable physical properties, the discrepancy between thin film materials and bulk materials has to be understood.

Various types of thin films deposition techniques have been used maturely in research and industry, such as chemical vapor deposition (CVD), physical vapor deposition (PVD), sputtering [1], but how thin film materials actually form on the surface of the substrate depends on various parameters, such as substrate materials, depositing materials, and deposition conditions [2]. There are three classical thin film growth modes, which are Frank-van der Merwe (FV), Volmer-Weber (VW), and Stranski-Krastonov (SK), and the growth mode determines the

thin film morphology, which in turn tailors its physical properties, such as resistivity and transmittance.

Because of the big lattice misfit, great surface energy difference, and some unexpected defects or contaminations between metal and oxide substrate, the thin metal film grows usually in the VW or SK mode [3]. Therefore, when the amount of as-deposited metal is very small and thickness is very thin, it is formed as discrete islands other than a continuous film. As the amount of metal deposited on the substrate is increasing, the film becomes continuous gradually [4, 5, 6]. Also, during the deposition process, the physical properties, particularly electrical and optical properties, are varying with the thickness of the deposited metal and the morphology of the thin film.

1.2. Transparency Conductive Oxides (TCOs)

Transparency conductive oxides (TCOs) are commonly used as electrodes in various types of optoelectronic devices, such as solar cells, liquid crystal displays (LCD), and organic light emitting devices (OLED), because they exhibit the high electrical conductivity and high optical transmittance [5].

1.2.a Popular TCOs

Currently, the most popular TCOs are indium tin oxide (ITO), which share the characteristics of low resistivity (~10^{-4} Ωcm) and high optical transmittance (85~90%) [7-8] in the visible region. However, the disadvantages of ITO are the

high cost and limited supply of indium, which leads to a lot of research and studies, attempting to find more cost-effective TCOs, yet with comparable electrical and optical properties.

Zinc oxide (ZnO) has received enormous attentions as a prospective candidate for ITO substitute in the optoelectronic devices, because it exhibits a wide band gap (~3.37 eV) and a large exciton binding energy (~60 eV), which makes it highly transparent in the visible region [9]; also, inexpensive and abundant materials sources could dramatically decrease the cost of transparent electrodes, and low toxicity makes it easy to recycle and store [6].

1.2.b Doping TCOs

ZnO is a semiconductor with excellent transparency, but the biggest challenge of ZnO is the high resistivity. Doping is a reasonable remedy for this problem, and recently aluminum (Al) and gallium (Ga) doped ZnO have reported relative low resistivity (~10^{-4} Ωcm) and high transmittance (~90%) [10, 11]. However, the limits are that complex doping process and how to determine the optimum doping composition could much complicate the manufacturing process and increase the cost, which brings more questions.

1.2.c TCO/Metal/TCO (TMT) Structure

Recently, a new method by inserting a metal layer between undoped TCOs forming a TCO-Metal-TCO (TMT) sandwich structure has gained a lot of

attentions [5, 6, 12]. This method can reduce the effective resistivity of the whole films by six orders, but the negative side is that since the inserted metal layer is not transparent, it will degrade the optical properties of TCOs. Therefore, in order to evaluate the overall performance of the TMT films including the optical and electrical properties, figure of merit (FOM) is introduced. Compared to doping method, only sputtering technique is required for the synthesis of TMT structure, which simplifies the fabrication process and decreases cost.

However, only a few metals can be the inserted layer and successfully tailor the electrical and optical properties of TCOs. Only silver (Ag), gold (Au), and copper (Cu) (mostly Ag and Au) have been documented that their TMT structures exhibit desirable FOM [6, 12, 13]. The reason is that when the deposited metal is in nano-particle structure, the incident light, an electromagnetic wave, penetrates in a certain depth of metal, where free electrons near the surface absorb and interact with the incident light, resulting in collective oscillation, known as surface plasmon polaritons (SPPs) [4]. As long as the frequency and wave vector of incident light and SPPs are in the proper range, resonance will occur and lead to constructive signals, which do not compromise the transparency of TCOs. Since the frequency and wavelength of SPPs are the intrinsic characteristics of metals, only for a few metals, they are in the desired range, such as Ag, Au, and Cu [14]. Therefore, these types of metals embedded TCOs systems can be considered as the candidates for the metal layer of TMT structure.

1.3 Thin Film Conduction Mechanism

As metal is deposited on the dielectric substrate at early stage and forms discrete metallic islands, the morphology shows small islands size and large spacing between metal islands, and the film exhibits large effective resistivity, which is categorized as dielectric zone. In this region, the film is well-known as negative temperature coefficient of resistivity (TCR), which is a typical property of semiconductor [4, 15]. As the deposited metal thickness is increasing, the islands start to coalesce with each other and form clusters, where it exhibits wide islands size distribution and more irregular shapes. In this regime, the resistance of the film exhibits a sharp drop, and this phenomenon is explained as percolation theory. This regime is defined as percolation zone [4, 15, 16]. When the metal thickness keeps increasing, the resistivity keeps decreasing and is close to the metallic resistivity. This region is designated as metallic zone [5, 6].

1.3.a Thermionic Emission

Before the metal film reaches the percolation critical thickness, the metal forms discontinuous islands on the dielectric substrate, where the whole film is highly resistive. Since the conduction mechanism in the ultra-thin film is very complicated, a lot of research and studies have been done in this field. Thermionic emission is one of the most-concerned mechanisms. The conduction mechanism of thermionic emission is that the electrons at the metal islands surface due to the heat-induced thermal energy overcome the barrier height caused by the difference of metal and insulator work function, and flow to the neighboring islands [17].

Due to the heat excited nature, thermionic emission is very temperature dependent, and is used in metal-semiconductor contacts [17-18].

1.3.b Tunneling

Tunneling is another most studied in thin film conduction mechanism. Because the general tunneling conduction mechanism is independent of temperature, which disobeys negative TCR characteristic, it has been dismissed for a long time. Until activated tunneling mechanism is discovered by Neugebauer and Webb [19], which fits well with the experimental data, tunneling conduction mechanism has been reconsidered as a dominant conduction mechanism in the thin film system. In terms of the general quantum mechanical tunneling theory, the tunneling current is determined by the number of electrons occupied the Fermi level, where it is able to pass through the barrier and the transmission coefficient, the probability that electrons actually penetrate the barrier. The mathematical expressions for quantum tunneling are in the function of inter-islands spacing, islands size, applied voltage, and other system intrinsic parameters [19-22].

The working mechanism of activated tunneling is generally the same as quantum mechanical tunneling, but the difference is that the tunneling electrons are not from the Fermi level, but from certain energy above the Fermi level. This amount of energy is designated as activation energy. The electrons cannot penetrate the barrier unless they are excited to the new energy level. The transmission coefficient of activated tunneling is also derived in terms of the

activation energy. Based on the Arrhenius equation, the activation energy is associated with temperature. Therefore, the effective resistivity of activated tunneling is related to the temperature, which successfully explains the phenomena of temperature dependent resistivity of the thin metal film system [19-22].

1.4 Electron Mean Free Path

Electron mean free path (EMFP) means the average travelling distance of a conducting electron between two subsequent collisions with lattices, defects, impurities, or boundaries, which can characterize the resistivity of materials. In bulk materials, the collisions of lattices, impurities, and defects play the major role of resistivity, but when the size of the materials is smaller than EMFP of corresponding bulk ones, the collisions begin to be dominated by the scattering between conducting electrons and materials boundaries. Therefore, as the thickness of the thin film is close to the EMFP of bulk metals or even smaller than it, the electrical properties of the thin films begin to behave differently from bulk ones. There are two main explanations of this phenomenon, which are interface scattering and grain boundary scattering [23-25]. Because the inserted metal layer in the TMT structure is only several nanometers thick, the resistivity of the system is anticipated to behave differently from the bulk one.

Chapter 2

EXPERIMENTAL PROCEDURE

2.1 Sample preparation

The flexible substrate materials used in the experiment was polyethylene napthalate (PEN) with thickness of 125 μm manufactured by Dupont Teijin Films, Melinex® with an adhesion promoting pretreatment on the film side. The silicon dioxide (SiO_2) and silicon (Si) glass substrates were also used in the experiments. Sliver (Ag) and zinc oxide (ZnO) were deposited on the PEN and glass substrates by using diode (DC) and radio frequency (RF) sputtering techniques respectively. Sputtering was performed using ZnO and Ag sputtering targets. The base pressure before deposition was approximately $1x10^{-7}$ Torr. Sputtering was carried out at a pressure of 10 mTorr in pure Ar. The thickness of the ZnO layer was fixed at 30 nm and Ag layers were varied between 2 and 10 nm in steps of 2 nm, which was verified by using Rutherford backscattering spectrometry (RBS).

2.1.a Direct Current (DC) Sputtering

The argon sputtering gas was injected into a chamber at a pressure of 10 mTorr, and then bombarded the Ag target. In the system shown in Fig. 2.1, negative potential was applied to the Ag target, which was acted as a cathode, so the ZnO substrate was performed as an anode. A certain fraction of the sputtered Ag atoms flew from the target to the substrate, and interacted energetically with the ZnO substrate. During this process, Ag thin film was formed at the surface of the ZnO substrate. This procedure is called the DC sputtering deposition

technique. During the DC sputtering, Ag layers were deposited on the ZnO and PEN substrate for 8/16/24/32/40 seconds corresponding to Ag thickness of 2/4/6/8/10 nm characterized by RBS technique.

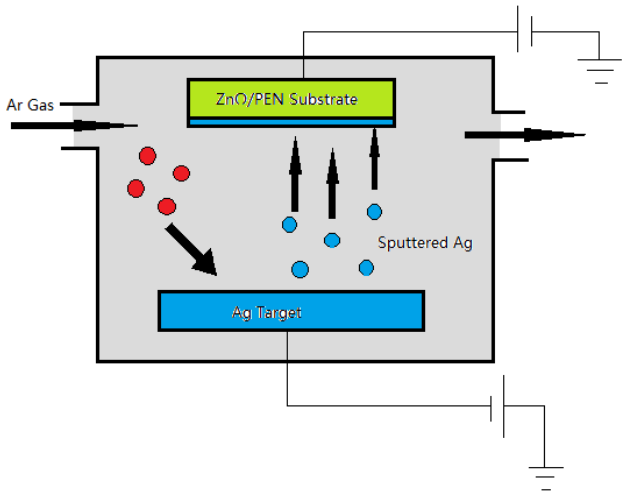

Fig. 2.1 Schematic of a DC sputtering instrumentation system

2.1.b Radio frequency (RF) Sputtering:

Dielectric materials or high resistivity semiconductors cannot be sputtered by using the conventional DC sputtering method, because charges would build up on the insulating target. Therefore, RF sputtering technique was introduced to sputter ZnO. In the RF sputtering system, the sign of the anode and cathode was alternating at a very high frequency, which avoided charges to accumulate on the ZnO target. Other than the alternating potentials, the deposition mechanism and the system of two sputtering techniques are the same. During the RF sputtering, the thickness of ZnO layer was fixed at 30nm. The setup of a typical RF sputtering is shown in Fig. 2.2.

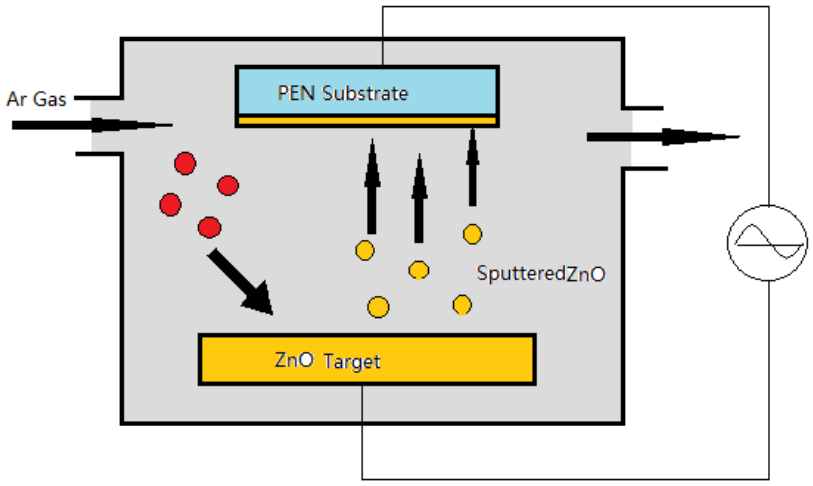

Fig. 2.2 Schematic of a RF sputtering instrumentation system

2.2 Materials Characterization

2.2.a Rutherford Scattering Spectrometry (RBS)

Rutherford backscattering spectrometry (RBS) is a non-destructive materials characterization technique. It was used to determine the thickness and composition of the Ag and ZnO thin film; also, it can be used to quantitatively characterize the depth profile, area density, and crystal lattice quality of the specimens [26]. A General Ionex Tandetron accelerator was used to generate helium (He) ion beam at energy of 2.0 MeV and total accumulated charge of 10 μC. Before the He ion beam entered the collimator to get focused, the incident ions were experienced a series of bending magnets, attempting to eliminate the unexpected particles based on their mass. After the mass selection process, ion beams entered the vacuum chamber under a pressure of 10^{-7} Torr, and then they "attacked" the specimens that were tilted 55^{o} off normal incidence and at a

scattering angle of 170^{o}. Samples and detector were in the Cornell geometry, which meant that the backscattering detector was directly under the incident beam. The backscattered ions were collected by a surface-barrier detector and analyzed with the aid of the RUMP computer-simulation program. Eventually, the RBS energy spectra were obtained by using the multichannel analyzer. The RBS system is shown in figure 2.3.

Since the sputtering deposition process cannot provide the information of the thin film thickness, RBS characterization technique was used to determine the thickness of ZnO and Ag thin film.

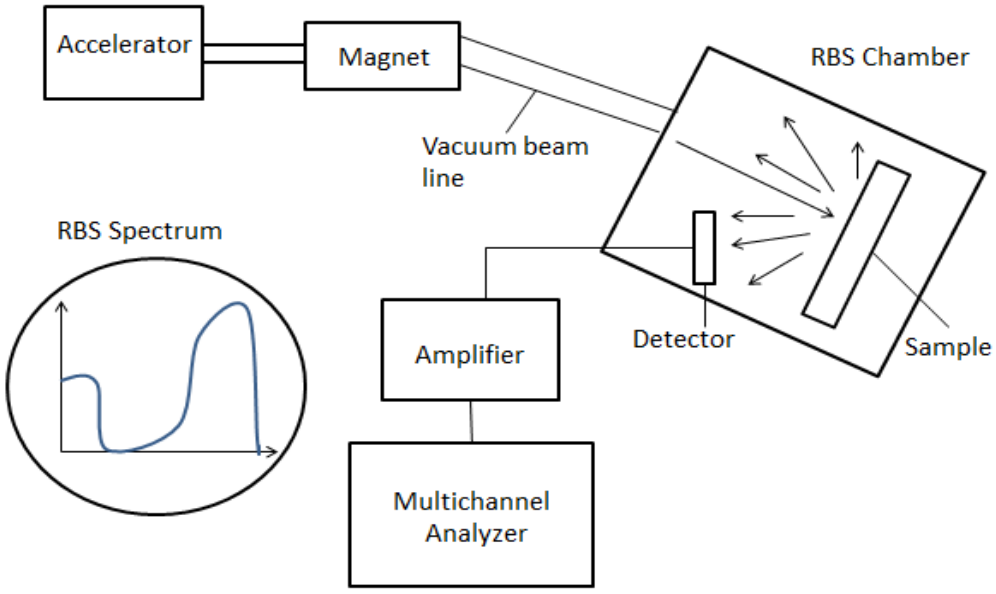

Fig. 2.3 Schematic of a Rutherford backscattering spectrometry instrumentation system

2.2.b Scanning Electron Microscopy (SEM)

Scanning electron microscopy (SEM) is mainly used to characterize the topography and composition of the samples. The schematic structure of a typical SEM is shown in the Fig. 2.4. An electron beam initially is emitted from an electron gun, and then focused by a series of condenser lenses. After passing through pairs of scanning coils or deflect plates, the primary electrons are deflected into the vacuum chamber and interact with the sample. During the interaction between incident beam and the samples, different types of electron are generated due to various types of scattering mechanisms, and then collected by different types of electron detectors. Secondary electrons are generated only near the surface, which is about the first 20nm from the sample surface. The distance is called escape length [26]. After secondary electrons leave the sample, they are detected by the secondary electron detector, which provides topography information. Backscattered electrons are originated from Columbic scattering of primary electrons, and the backscatter electron detector collects them, which gives composition of the samples. X-rays and transmitted electrons are also detected by specific detectors offering other information. The schematic diagram of the interaction between primary electrons and samples is shown in Fig. 2.5.

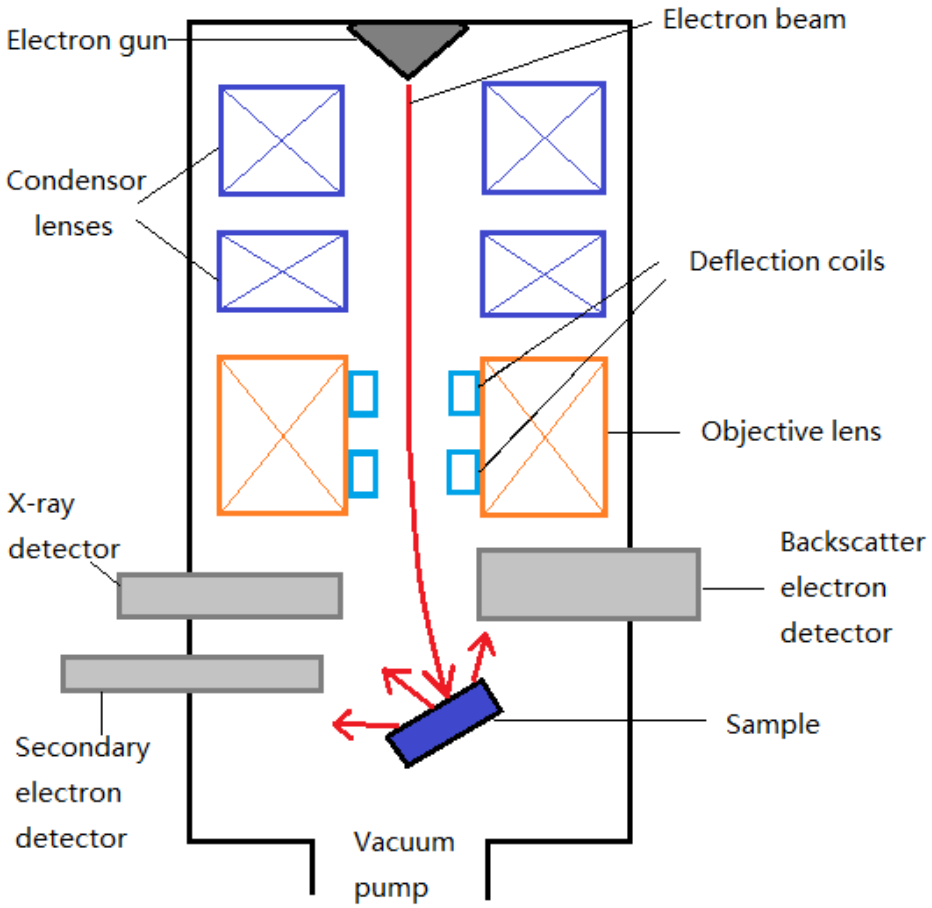

Fig. 2.4 Schematic of a scanning electron microscopy instrumentation system

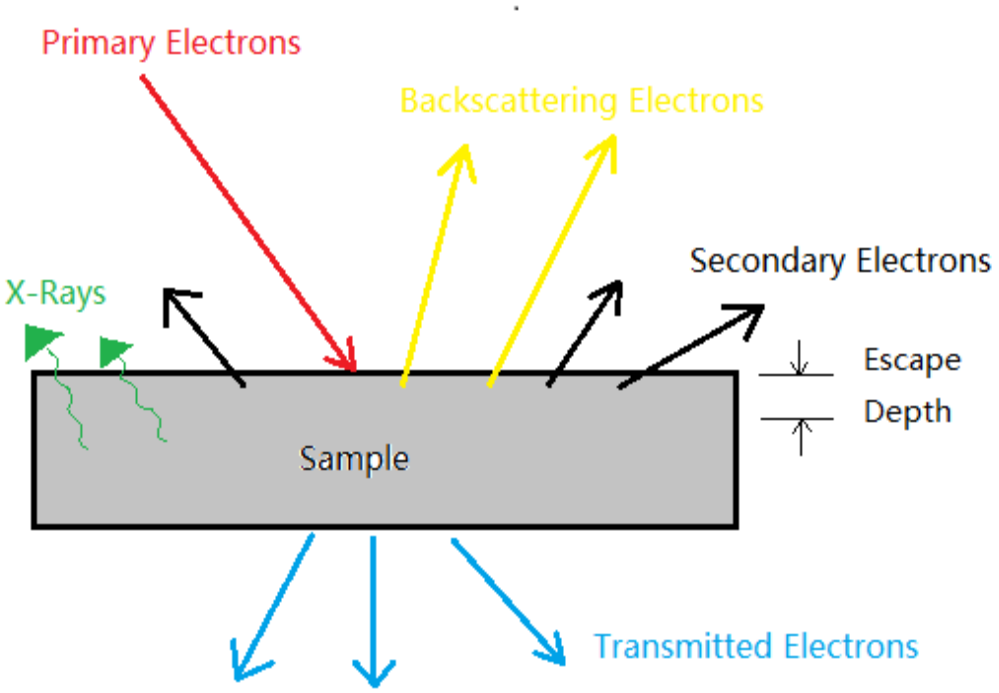

Fig. 2.5 Different types of scattered electrons after the primary electron beam interacted with the sample in the SEM

In the experiment, SEM was used to characterize the morphology of the Ag film, such as Ag islands size, inter-islands spacing, and Ag surface coverage, which were essential parameters for the thin film research due to the fact that Ag cannot form continuous film when the Ag thickness was very thin, which affected the electrical and optical properties of the thin film system.

Figure 2.6 Philips XL 30 scanning electron microscopy used at ASU (Courtesy: CSSS，ASU)

2.2.c Hall Measurements

In attempt to determine the resistivity and mobility of the thin film samples with respect to different Ag thickness, Hall effect measurement was performed over the samples. Before performing the Hall measurement, the samples were mounted onto a printed circuit board by using copper wires and silver paste to establish the contacts.

The Van der Pauw method is commonly used to characterize various electrical properties of semiconductors, such as resistivity, mobility of carriers, and carrier concentration. In order to implement Van der Pauw method and reduce errors, the samples were cut into square shape, $1x1cm^2$. In order to make

good Ohmic contact, sliver paste was used to make contacts at the four corners of the square samples, and then the silver and printed circuit board were connected by copper wires. The configuration of the Hall measurement samples was shown in Fig. 2.6. In the figure, the contacts were numbers from 1 to 4 in a clockwise direction. Initially, the current was flown into contact 1 and out of contact 2, and voltage was measured across contacts 3 and 4. After first measurement, the current again circulated from contact 2, out of contact 3, and the voltage was measured across contacts 1 and 4.

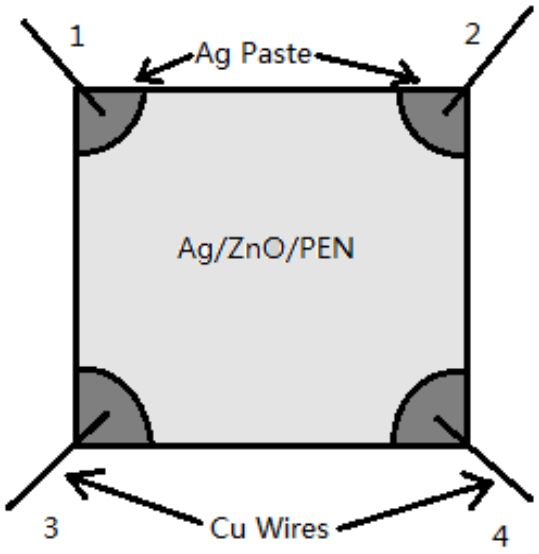

Fig. 2.7 Hall measurement sample labeled for the contacts.

The average of ratios of the voltage V_{34} and I_{12}, and V_{14} and I_{23} gave the resistance of the sample.

$$R_{12,34} = \frac{V_{34}}{I_{12}} \quad (1)$$

$$R_{23,14} = \frac{V_{14}}{I_{23}} \quad (2)$$

$$R = \frac{1}{2}(R_{12,34} + R_{23,14}) \quad (3)$$

The resistivity of the whole film

$$\rho = \frac{\pi t}{\ln 2} FR \text{ [27]} \quad (4)$$

Where t=the thickness of the ZnO and Ag

F=correction factor depending on the size of the sample.

The resistivity is measured by the Vρ shown in Fig. 2.7. The voltage drop over the distance of s is measured, and divided by the current flowing through the system, so the resistance can be known. Since the length and the cross section area are already known according to the setup specifications, the resistivity of the sample can be measured given

$$\rho = \frac{dw}{s}\frac{V_\rho}{I} \quad (5)$$

Where d=The width of the setup

w=The height of the setup

s=The distance between the Vρ and ground

I=Current

Vρ=The voltage drop

In the Hall measurement system, the electrons experience a magnetic field and a force known as Lorentz force is exerted on them, which causes them to deflect from the initial direction. In the Hall measurement setup shown in Fig. 2.7,

the magnetic field was perpendicular to the motions of the electrons, and hence the force can be expressed as

$$\vec{F} = q(\vec{v} \times \vec{B}) = qvB \quad (6)$$

Where q=The charge of the conducting particles in the unit of coulombs (C)

v=Velocity of electrons

B=The strengthen of the magnetic field in the units of Wb/cm^2

The Lorentz force deflects the electrons and causes them to accumulate on the bottom of the setup, which in turn induces an electric field. The force induced by electric field could offset the Lorentz force. When the two forces cancel out, the voltage across the setup is called Hall voltage, V_H, given by,

$$V_H = \frac{BI}{qdn} \quad (7)$$

Where d=the width of the material.

n=the electrons concentration in the material

In order to further understand this topic, Hall coefficient is introduced, given by

$$R_H = \frac{dV_H}{BI} \quad (8)$$

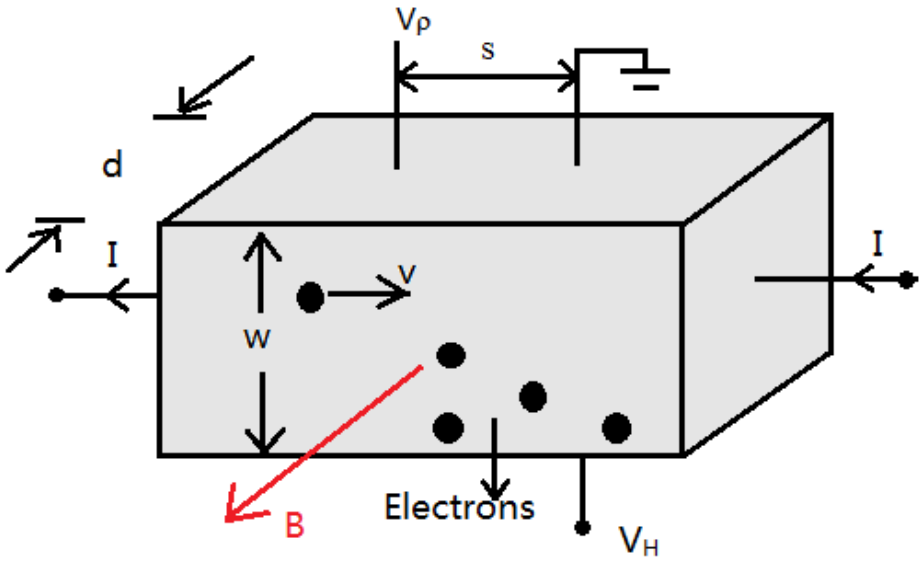

Fig. 2.8 Function mechanism of Hall measurement system

The carrier concentration can be expressed as,

$$n = -\frac{r}{qR_H} \tag{9}$$

Where r=Hall scattering factor, which is around 1~2.

Mobility was given

$$\mu_H = \frac{R_H}{\rho} \tag{10}$$

Where ρ=resistivity

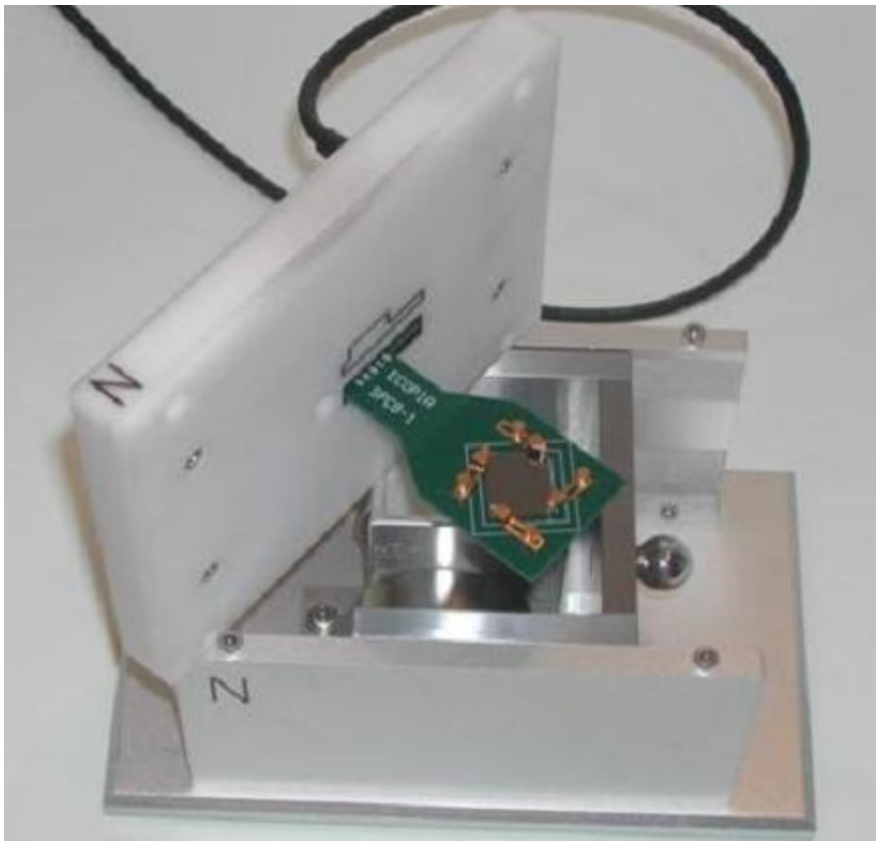

Fig. 2.9 Ecopia HMS-3000 Hall Effect Measurement System used at ASU (Courtesy: ASU)

2.2.d Four Point Probe Measurement

The sheet resistance, which is one of the most important parameters in the semiconductor area, was measured by using a typical in line four-point configuration as shown in the Fig. 2.9, and the four probes have been numbered from 1 to 4. Current was flowing from the probe 1, and out of probe 4, but the voltage drop was measured between probe 2 and 3. The reason using this setup is to avoid the influence of probe wire resistance (R_{Probe}), contact resistance ($R_{Contact}$), and probe spreading resistance ($R_{Spreading}$) [27], which could be introduced by the two terminals measurements, shown in Fig. 2.10. However, all these parasitic

resistances can be neglected by using the four point probe setup, because the voltmeter has extremely high impedance, which causes very little current passing through the probe 2 and 3. Therefore, the voltage reading from the voltmeter across probe 2 and 3 does not come from the parasitic resistances mentioned above, but almost entirely from the semiconductor sheet resistance under these two probes.

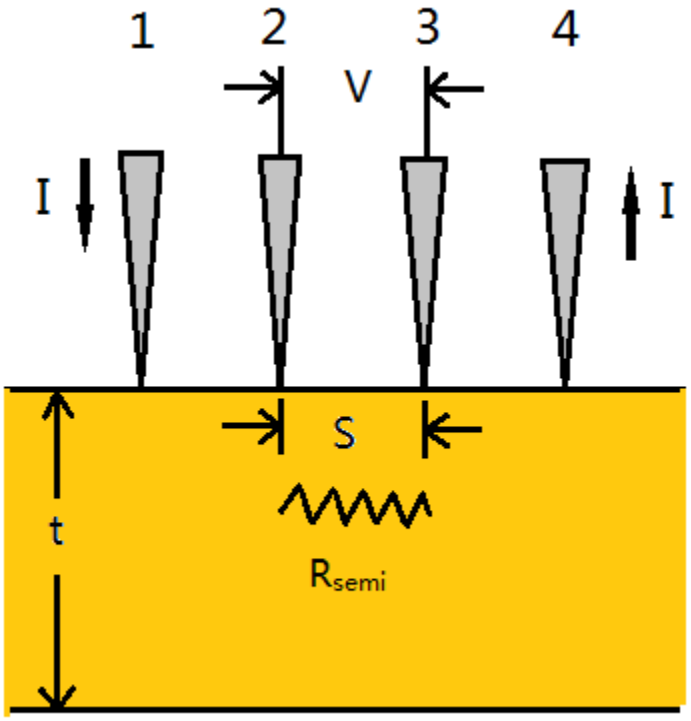

Fig. 2.10 Layout of a typical four point probe setup. Measurements taken at ASU had a probe spacing of 2 mm. Where s=spacing between the probes and t=the thickness of the sample.

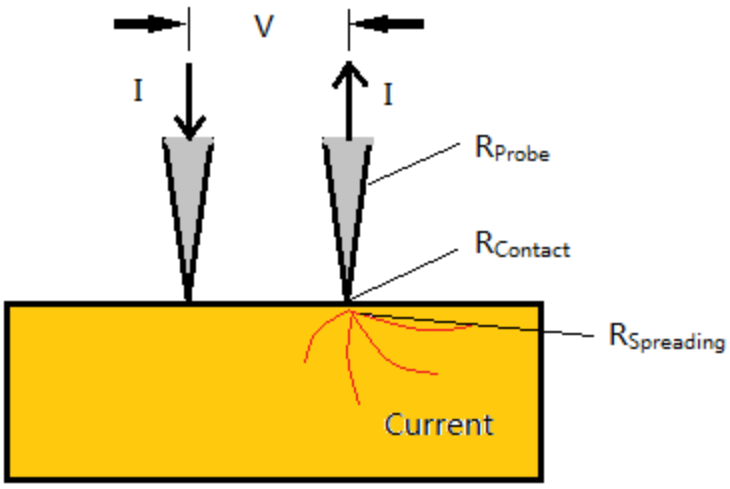

Fig. 2.11 Schematic of various types of resistance at the tip of the probe

The sheet resistance is calculated from the measured values, which is the ratio of the voltage to the current, and multiplying by the correction factor depending on the actual sizes of the samples, such as probe spacing, the width and length of the samples. The sheet resistance is expressed as follows,

$$R_{sh} = \frac{V}{I} \times CF \quad (11)$$

Where CF=correction factor

V/I=the reading from the monitor. V is the voltage drop across probe 2 and 3, and I the current passing through the samples.

The resistivity of the samples can be calculated by using the following expression, given by:

$$\rho = R_{sh} \times t \quad (12)$$

Chapter 3

SIMULATION OF EVOLUTION OF CONDUCTION MECHANISM IN THIN FILM SILVER ON ZINC OXIDE

3.1 Introduction

It has been reported that the TMT structure can significantly improve the electrical property of intrinsic TCOs without compromising the transparency too much, which yields comparable Figure of Merit (FOM) [5, 6, 12]. Specifically, as the thickness of middle metal layer increases, the effective resistivity of the TMT film decreases dramatically starting from a critical thickness, and then gradually approaches to a certain value. There are a lot of studies and research in terms of thin metal film conduction mechanism, but some of them are only science-based investigation without implementing actual applications; yet, others only explain the phenomena without touching the fundamental theory. Therefore, this work combined the fundamental theory and actual applications.

Due to the cost issue of ITO, ZnO has become a very promising TCO candidate, and the ZnO/Metal/ZnO structure has been proved as a feasible solution [6, 28]. However, since there is another ZnO layer on top of the system, it is difficult to investigate the structural and electrical properties at the interface, where it could play an important role to determine the various properties of the whole system. Therefore, the top ZnO layer is removed, and Ag/ZnO film samples are prepared by using DC and RF sputtering respectively. It turns out that this method offers a better view of the interface morphology.

3.2 Literature Background

As mentioned above, with the evolution of the Ag film thickness, the whole film has been categorized into three regimes based on the electrical characteristics, which are dielectric zone, percolation zone, and metallic zone. The anticipated evolution of Ag film morphology is shown in Fig. 3.1. Initially, in the dielectric zone, as the thickness of the Ag is very thin, the islands size (r) is relatively small, but the spacing between islands is large. With the processing of sputtering, there are more sputtered Ag and the islands size (r) is expanding, but contrarily the spacing (s) shrinks. When discontinuous islands begin to interconnect each other and Ag clusters are formed, the conducting electrons are able to move from one island to another one freely without passing huge ZnO barrier. Once there is a giant cluster that percolates the whole system, the effective resistivity of whole film exhibits an enormous drop and begins to show the characteristics of metallic materials. It is recognized as percolation zone. As the Ag grows thicker, islands size begins to expand even larger, and neighboring islands begin to overlay each other. The Ag film becomes continuous gradually, and the effective resistivity is decreasing gradually and approaches to a value close to the bulk Ag. The side view of the morphology evolution of Ag film is shown in Fig. 3.2.

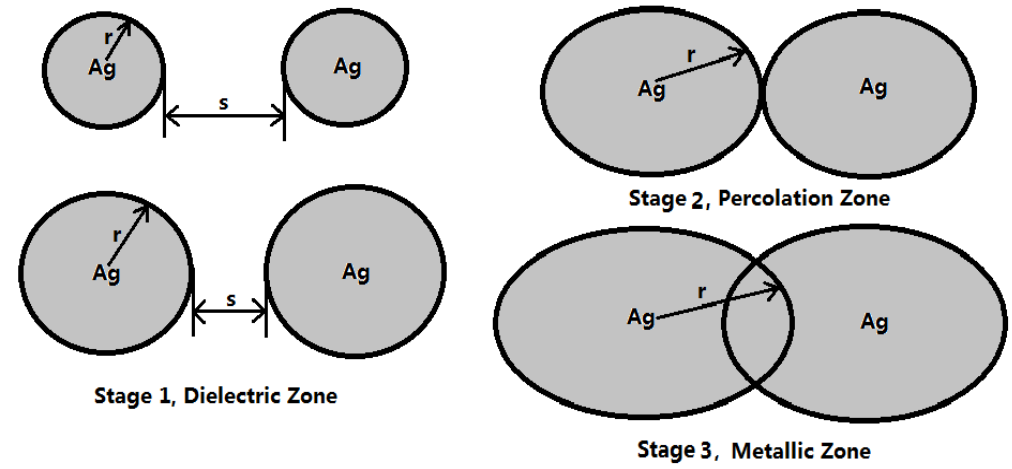

Fig. 3.1 The top view of three stages of electrical characteristics of Ag/ZnO thin film system with respect to the evolution of Ag morphology

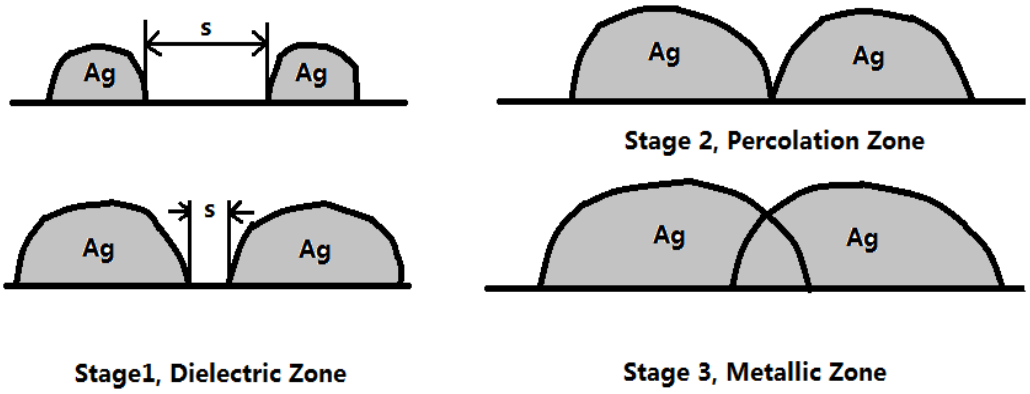

Fig. 3.2 The side view of three stages of electrical characteristics of Ag/ZnO thin film system with respect to the evolution of Ag morphology

3.2.a Dielectric Zone

At the beginning of the sputtering process, only a small amount of Ag is sputtered on the ZnO surface, due to the thin film growth mechanism as mentioned above, the Ag film forms discrete islands other than continuous film. Therefore, the morphology of the Ag film is that small Ag islands are separated by large ZnO gaps.

The ZnO used in this work is an intrinsic semiconductor (99.99% of pure ZnO), so it could be regarded as a layer of dielectric material with thickness of 30 nm. Since the ZnO film is deposited by using RF sputtering technique, the structure of ZnO film is polycrystalline, and it grows preferentially in the direction perpendicular to the substrate [29-31]. The resistivity of ZnO thin film varies a lot depending on a number of factors, such as the deposition rate, crystal orientation, and various experimental conditions [30-32]. It has been documented that the ZnO film resistivity varies from 10^3 to 10^9 Ωcm [29-32]. Due to the high resistivity of ZnO film and discontinuous Ag morphology, the Ag/ZnO film exhibits high resistivity as well, which is a typical characteristic of dielectric material. Therefore, Ag/ZnO film in this stage is categorized as dielectric zone.

However, since there is a thin layer of Ag on top of ZnO film, it is estimated that the electrical behavior of the Ag/ZnO film cannot be exactly the same as that of pure ZnO film. According to the morphology of thin Ag film sputtered on ZnO shown in Fig. 3.1 and 3.2, if there is a current flowing across the film, two Ag islands can regarded as two electrodes separated by ZnO medium, which is a metal-insulator-metal (MIM) structure; also, it can be considered as two metal-intrinsic semiconductor contacts conjoint each other [17-18]. Based on the current transport theory of Schottky barrier diodes, there are two major conduction mechanisms, which are thermionic emission and tunneling [17, 18, 27].

3.2.b Thermionic Emission

Thermionic emission is a conduction mechanism caused by the electrons near the metal surface. When the energy of electrons is higher than the effective barrier height resulting from the difference of metal and semiconductor work function, they can overcome the barrier and transmit to the neighboring metal island. Due to the fact that the work function of Ag (~4.4 eV) is smaller than that of ZnO (~5.2 eV) [9] shown in Fig. 3.3, when Ag and ZnO are brought into contact and all Fermi levels line up, ideally the electrons from the Ag inject into ZnO, and two accumulation type of contacts are formed shown in the Fig. 3.4.

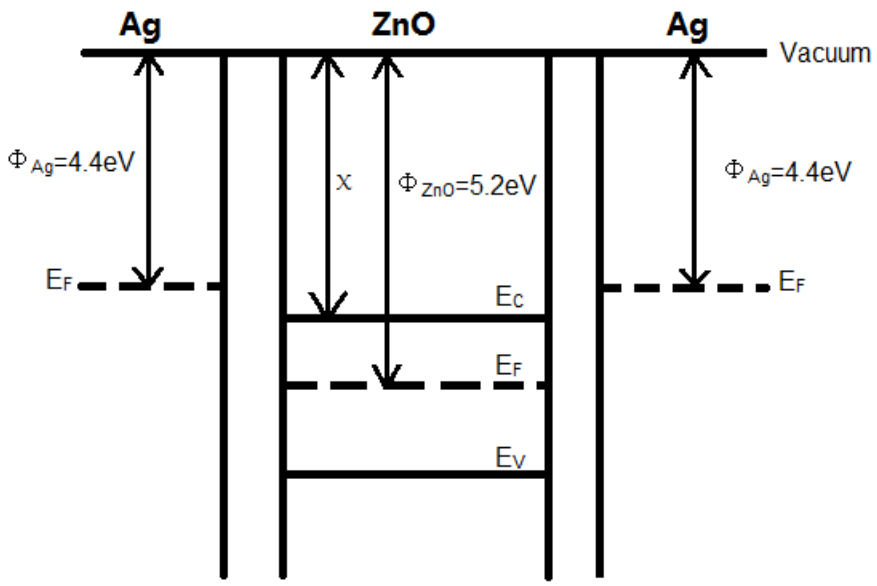

Fig. 3.3 The Energy band diagram of Ag/ZnO/Ag structure before brought into contact and the vacuum energy levels line up

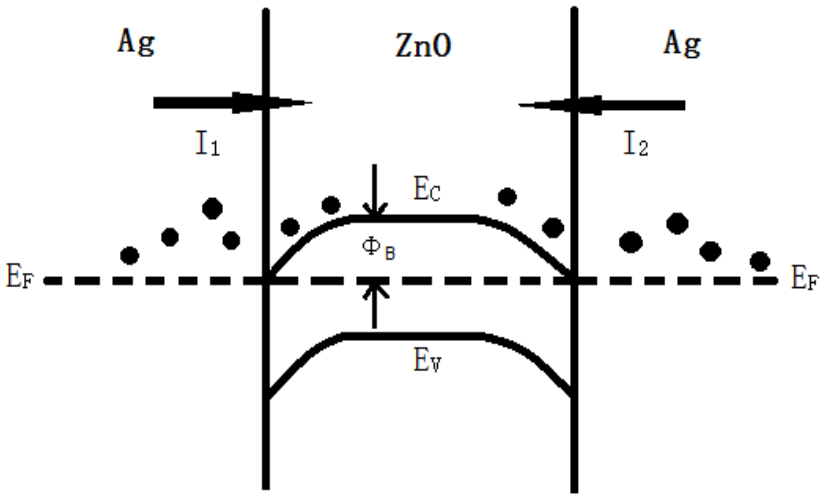

Fig. 3.4 The energy band diagram of Ag/ZnO/Ag structure after brought into contact and the Fermi levels line up

Based on the MIM structure shown in Fig. 3.4, there will be no net current, because the currents caused by injected electrons from both sides are in the same magnitude and balance out. In order to have net current flowing, an applied voltage (V) is required. When the voltage is applied across two Ag "electrodes", the symmetric barrier shape will be changed, so the electrons from both sides need to overcome different barrier heights to flow from one side to another, where net current can be yielded. The new MIM structure when the applied voltage and image force are considered is shown in Fig. 3.5. Due to the applied voltage, the Fermi level in the right side of Ag is lowered by "eV", so the ZnO barrier shifts down by eV as well. If the image force is taken into account, it can round off the corners and reduce the barrier height [33-35], which is shown in Fig. 3.5.

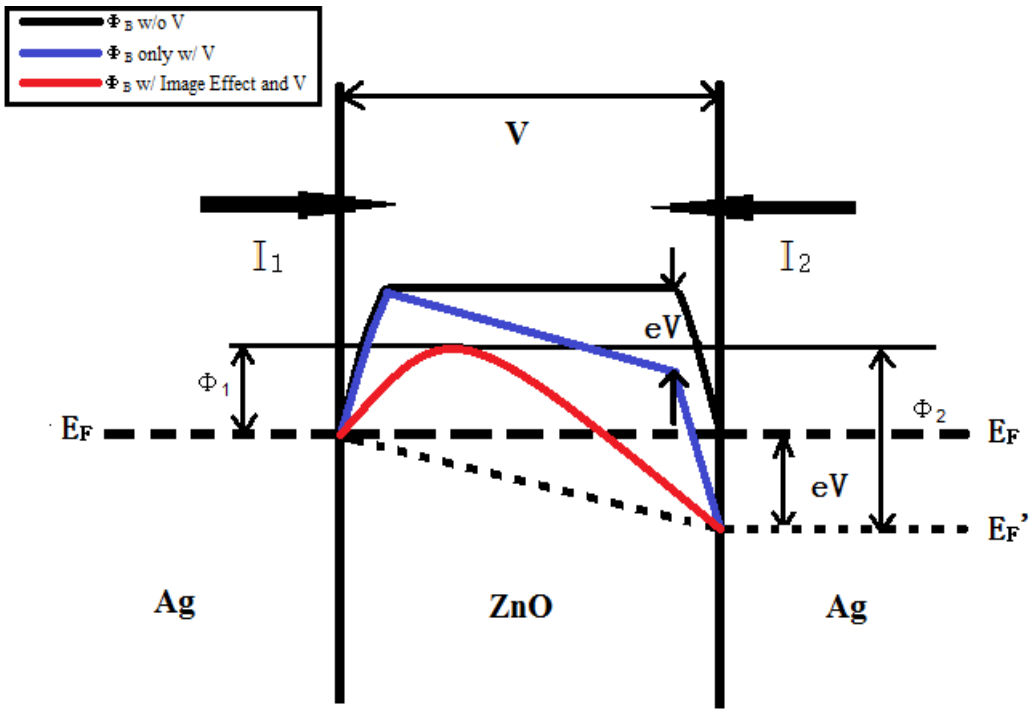

Fig. 3.5 The effective ZnO barrier height without considering the applied voltage (black), only considering the applied voltage (blue), and considering both applied voltage and image force effect (red)

According to the Schottky barrier diode theory, the current-voltage characteristic is described as Richardson-Dushman equation [17]

$$J = \frac{4\pi m_n^* q k^2}{h^3} T^2 \exp\left(\frac{-\Phi}{kT}\right) = A^* T^2 \exp\left(\frac{-\Phi}{kT}\right) \quad (1)$$

Where J=current density

h=Planck constant=6.63×10^{-34} (Js)

k=Boltamann constant=1.38×10^{-23} (J/K)=8.62×10^{-5} (eV/K)

q=1.6×10^{-19} C

T=Room temperature=300 K

$m_n^* = 0.25m_0$=the electron effective mass in the ZnO [36]

m_0=9.1×10^{-31} kg

Φ=Barrier height

$A^* = \frac{4\pi m_n^* q k^2}{h^3} = 34.66\ (A/cm^2K^2)$

The current density flowing from left to right is denoted as J_1, and from right to left is expressed as J_2, so the net current density is given by

$$J_{net} = J_1 - J_2 = A^*T^2[\exp\left(-\frac{\Phi_1}{kT}\right) - \exp\left(-\frac{\Phi_2}{kT}\right)] \quad (2)$$

Where Φ_1 and Φ_2 = The barrier heights shown in the Fig. 3.5

The relationship of Φ_1 and Φ_2 is given

$$\Phi_2 - \Phi_1 = eV \quad (3)$$

Where $e=1.6x10^{-19}$ C

V=The applied voltage across the ZnO barrier, and value of V depending on the experimental conditions.

Therefore, the overall expression is given

$$J_{net} = A^*T^2\exp\left(-\frac{\Phi_1}{kT}\right)[1 - \exp\left(-\frac{eV}{kT}\right)] \quad (4)$$

Here only Φ_1 is unknown. In order to require more accurate Φ_1, not only should difference of work function be considered, both applied voltage and image potential also need to take into consideration.

Simmons [35] came up with the general equation of effective barrier height including the applied voltage and image potential, which is given

$$\Phi = \Phi_0 - \frac{0.36}{Kx} - (\frac{0.7}{Ks} + eV)\frac{x}{s} \quad (5)$$

Where Φ_0=The initial work function difference between Ag and ZnO=5.2-4.4=0.8 eV

K=Dielectric constant of ZnO=8.7 [36]

s=Separation between two neighboring Ag islands in unit of nm

x=The distance from the left Ag/ZnO interface ranging from 0 to s in unit of nm

Since Φ_1 is the maximum barrier height, in an attempt to find Φ_1, the derivative of equation 5 sets equal to zero and solve x. The result of x is given

$$x_0 = s\left(\frac{0.36}{0.7+eVKs}\right)^{\frac{1}{2}} \quad (7)$$

Substitute x_0 in equation 5 gives

$$\Phi_1 = \Phi_0 - \frac{1.2}{Ks}(0.7 + eVKs)^{\frac{1}{2}} \quad (8)$$

Where Φ_1 is in unit of eV.

Therefore, the net current density can be expressed as

$$J_{net} = A^*T^2 \exp\left(-\frac{\Phi_0 - \frac{1.2}{Ks}(0.7+eVKs)^{\frac{1}{2}}}{kT}\right)\left[1 - \exp\left(-\frac{eV}{kT}\right)\right] \quad (9)$$

3.2.c Tunneling

Based on the Schottky theory, tunneling is another dominant current-voltage characteristic of metal-semiconductor contact, especially when the two electrodes are very close [27]. The tunneling current-voltage characteristic is caused by the tunneling movement of the electrons close to the Fermi level from one island to another one shown in Fig. 3.6. However, only a fraction of them can actually penetrate the ZnO barrier, which is designated as transmission coefficient, D.

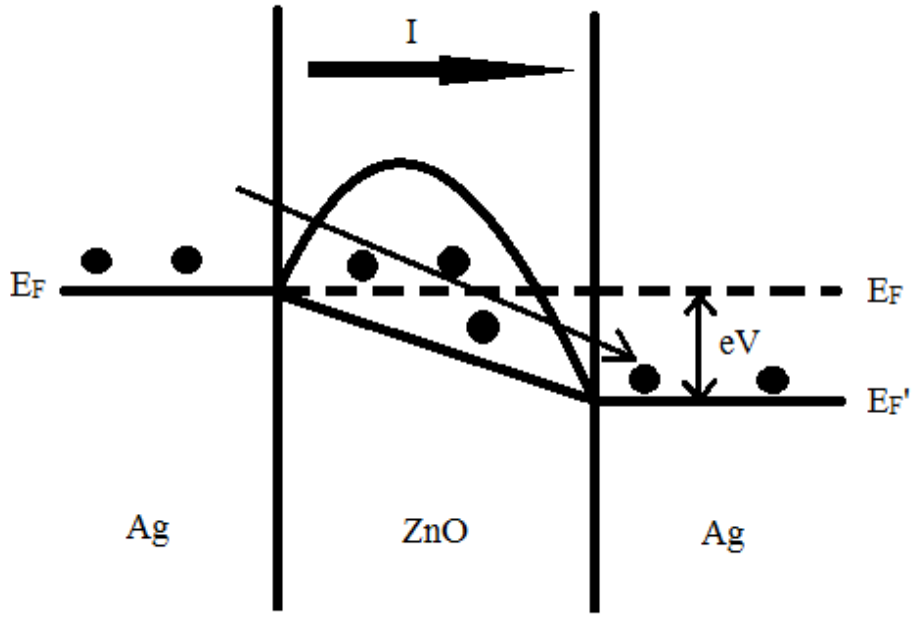

Fig. 3.6 The electrons near the Fermi level in left side Ag tunnel through the ZnO barrier and reach the new Fermi level in the right side Ag based on the quantum mechanical tunneling theory.

The general tunneling current density is given

$$J = NxD \tag{10}$$

Where N=the number of electrons per cm^2 close to the Fermi level

D=transmission coefficient

Firstly, quantum mechanical tunneling is studied. Assumed that electrons in the Ag electrode are isotropic distributed, there is a certain number of quantum states in a unit volume, which correspond to the certain values of momenta given by [37]

$$p_x = \frac{hn_x}{a_x};\ p_y = \frac{hn_y}{a_y};\ p_z = \frac{hn_z}{a_z} \tag{11}$$

Where p_x, p_y, p_z=Components of electron momentum

h=Planck's constant

n_x, n_y, n_z=Integers involved in solution wave equation

a_x, a_y, a_z=dimensions of potential well

Therefore, at a specific energy state ($n_{x,y,z}$=1), only unit volume is considered ($a_{x,y,z}$=1), the momentum space per unit volume is $h^3/2$, where 1/2 counts for the positive and negative spins. Based on the assumption above, the quantum states per unit volume is expressed as

$$\frac{m^3 dV_x dV_y dV_z}{\frac{h^3}{2}} = \frac{2m^3 dV_x dV_y dV_z}{h^3} \quad (12)$$

Where V_x, V_y, V_z=Components of electron velocity

m=The mass of an electron

$m^3 dV_x dV_y dV_z$=Elemental volume

Among those quantum states, a certain number of them is occupied by electrons, which is denoted as f(E), so the total number of electrons per unit volume in Ag is given

$$\iiint_{-\infty}^{\infty} \frac{2m^3}{h^3} f(E) dV_x dV_y dV_z \quad (13)$$

Since the transmission coefficient determines how many electrons actually penetrate the ZnO barrier, the total number of tunneling electrons in direction of tunneling is expressed as

$$J = \iiint_{-\infty}^{\infty} \frac{2m^3}{h^3} f(E) D(E_x) V_x dV_x dV_y dV_z \quad (14)$$

Where E_x=Component of electron energy in direction of tunneling

Based on the conversion from Cartesian coordinates to polar coordinates, the total quantum mechanical tunneling current density is given by

$$J = \frac{4\pi me}{h^3}\int_0^{\Phi 1} D(E_x)dE_x \int_0^{\infty}[f(E) - f(E + eV)]dE_r \qquad (15)$$

Where Φ_1=the maximum barrier height

E_r=Radial component of electron energy in a plane at right angles to tunneling.

In order to solve the total current density, the transmission coefficient has to be solved. In Simmons work [33-35], the transmission coefficient is given by

$$D(E_x) = \exp[-A{\Phi_1}'^{\frac{1}{2}}]\exp[-B(E_F - E_x)] \qquad (16)$$

Where $A = \frac{4\pi s}{h}(2m_n^*)^{1/2}$ ($J^{-1/2}$)

s=The separation between two neighboring Ag islands in unit of nm

$B = A/2{\Phi_1}'^{1/2}$ (J^{-1})

${\Phi_1}'$=Maximum barrier height in unit of Joules=$q\Phi_1$

E_F=Fermi energy level

Substitute equation 16 to 15 and integrate the whole equation, and it turns out the overall current density equation is given by

$$J(V,T) = \frac{4\pi mq}{h^3B^2}\frac{\pi BkT}{\sin(\pi BkT)}\exp\left(-A{\Phi_1}'^{\frac{1}{2}}\right)[1 - \exp(-BqV)] \quad (17)$$

Where kT=8.62x10^{-5}x300 (eV)=0.02586 (eV)

q=1.6x10^{-19} C

V=applied voltage in unit of V

Because the term $\frac{\pi BkT}{\sin(\pi BkT)}$ can be approximated to $\frac{1}{1-\frac{1}{6}(\pi BkT)^2}$, which is derived from the Taylor series of $\sin x = x - \frac{x^3}{3!} + \frac{x^5}{5!}\cdots$, the overall current density of quantum mechanical tunneling is expressed as

$$J(V,T) = \frac{4\pi mq}{h^3 B^2} \frac{1}{1-\frac{1}{6}(\pi BkT)^2} \exp\left(-A{\Phi_1}'^{\frac{1}{2}}\right)[1-\exp(-BqV)] \quad (18)$$

Although there is a temperature term in equation 18, it shows that the current density of quantum mechanical tunneling is insensitive to the temperature. However, it is reported that the thin metal film exhibits negative temperature coefficient of resistance, which means the resistivity decreases as the temperature increases [19], so the quantum mechanical tunneling theory is not sufficient enough to explain the whole current voltage characteristics in thin metal film sputtered on dielectric materials.

A new tunneling mechanism, which is called activated tunneling, was proposed by Neugebauer and Webb [19] in 1962. Since initially the energy level, where tunneling electrons come from, is considered as the Fermi level, but in the newly-proposed theory, the tunneling level is certain amount of energies beyond the original Fermi level, due to the reasons that it is necessary to supply certain amount of energy when an electron is transferred from one neutral island to another one suggested by Gorter [38] and Darmois [39]. The certain amount of energy is designated as activation energy, δE shown in Fig. 3.7.

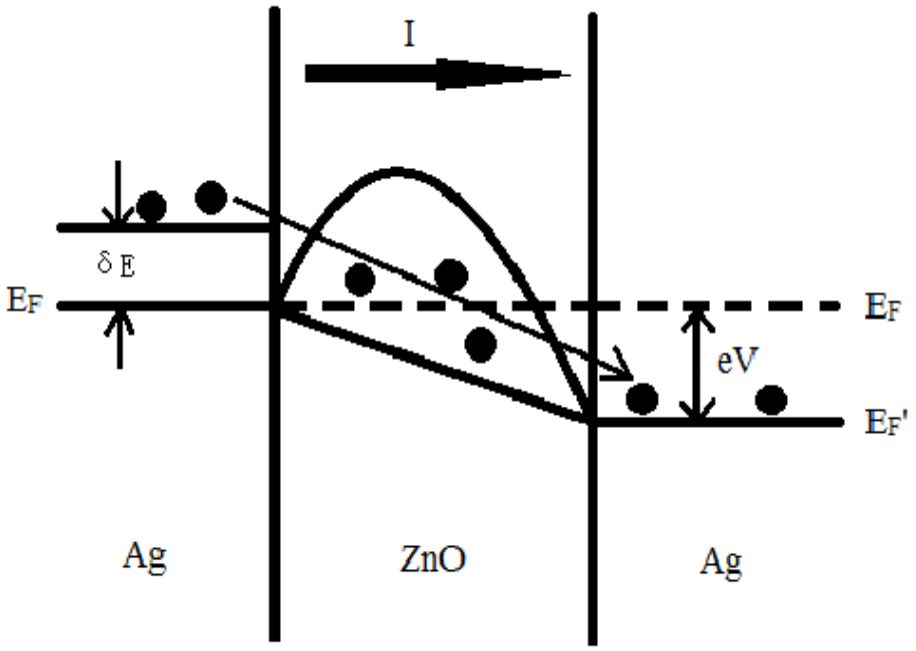

Fig. 3.7 The electrons at the energy level δE above the original Fermi level in the left side Ag tunnel through the ZnO barrier and reach the Fermi level in the right side Ag based on the activated tunneling theory

In order to tunnel through the barrier, the "qualified" electrons have to be elevated δE above the Fermi level, and the activation energy is given [19, 40]

$$\delta E = \frac{e^2}{4\pi\varepsilon_0\varepsilon_r}\left(\frac{1}{r} - \frac{1}{r+s}\right) \text{ (eV)} \qquad (19)$$

Where ε_0=The permittivity of vacuum=8.854x10^{-12} (F/m)

ε_r=The relative permittivity=$p\varepsilon_0 + (1-p)\varepsilon_{ZnO}$

ε_{ZnO}=The permittivity of ZnO=8.7ε_0 [36]

p=The area coverage of Ag on the ZnO

r=The mean Ag island radius in unit of nm

s=The separation between neighboring islands in unit of nm

Taking into account the Boltzmann statistics, the total number of electrons that can tunnel through the barrier is given by [37]

$$n = N\exp(-\frac{\delta E}{kT}) \quad (20)$$

Where N=The number of electrons tunneling electron at the Fermi level

Hill [20] included the activation energy in the transmission coefficient, and derived the general equation for current density of activated tunneling. Since the general equation is extremely complicated, he made some approximation based on the relationship between activation energy, δE and kT. When the δE is bigger than kT, the current density is approximated as

$$J = \frac{8\pi mq}{h^3B^2}\sinh\left(\frac{eV}{kT}\right)\frac{\pi BkT}{\sin(\pi BkT)}\exp\left(-A{\Phi_1}'^{\frac{1}{2}}\right)\exp\left(\frac{-\delta E}{kT}\right)[1-\exp(-BqV)] \quad (21)$$

Where $A = \frac{4\pi s}{h}(2m_n^*)^{1/2}$ ($J^{-1/2}$)

s=The separation between two neighboring Ag islands in unit of nm

$B = A/2{\Phi_1}'^{1/2}$ (J^{-1})

${\Phi_1}'$=Maximum barrier height in unit of Joules=$q\Phi_1$

kT=8.62x10^{-5}x300 (eV)=0.02586 (eV)

m=The mass of an electron

q=1.6x10^{-19} C

V=applied voltage in unit of V

As mentioned above the term $\frac{\pi BkT}{\sin(\pi BkT)} \approx \frac{1}{1-\frac{1}{6}(\pi BkT)^2}$, the equation is written by

$$J = \frac{8\pi mq}{h^3 B^2} \sinh\left(\frac{eV}{kT}\right) \frac{1}{1-\frac{1}{6}(\pi BkT)^2} \exp\left(-A{\Phi_1}'^{\frac{1}{2}}\right) \exp\left(\frac{-\delta E}{kT}\right) [1 - \exp(-BqV)] \quad (22)$$

WhenδE is smaller than kT, the current density is approximated as

$$J = \frac{8mq}{h^3 B^2} \sinh\left(\frac{eV}{kT}\right) \frac{(\pi BkT)^2}{\sin(\pi BkT)} \exp\left(-A{\Phi_1}'^{\frac{1}{2}}\right) [1 - \exp(-BqV)] \frac{kT}{\delta E} \quad (23)$$

Since kT equals to 0.0258eV at room temperature, and activation energy is $0.303\left(\frac{1}{r} - \frac{1}{r+s}\right)$ eV, assumed the Ag area coverage is 50%. When the Ag film is in the dielectric regime, the "r" is relative small, but "s" is larger than "r". Thus, practically the activation energy is always larger than kT at room temperature, so the equation 22 is the current density expression used in following studies and research.

3.2.d. Percolation Theory

Percolation theory is a model that can explain the electrical characteristics phase transition of Ag/ZnO film from dielectric materials to metallic materials; also, it is a theory that can relate occupation probability to the morphology of the sputtered islands.

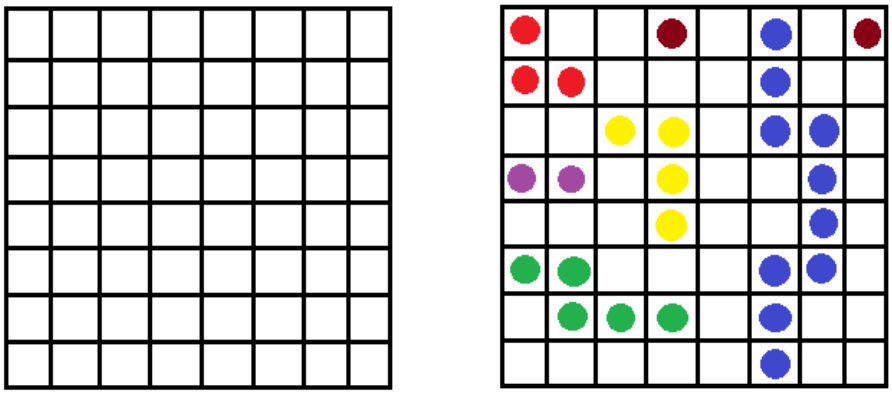

Fig. 3.8 (a) shows a 8x8 square lattice that can be regarded as ZnO film (b) the different colored dots indicate the sputtered Ag that have been grouped into certain clusters, and the blue cluster represents the percolating cluster

In Fig. 3.8 (a), the 8x8 square lattices can be regarded as the ZnO film before Ag sputtering, and the dots sitting on the square lattices in Fig. 3.8(b) are the sputtered Ag islands. When two unit squares occupied with dots are neighbored each other, more specifically, the edges of two squares are touched (not the corners), they can be grouped into a cluster. Thus, in Fig. 3.8(b), there are 7 clusters totally. 2 clusters that only contain one individual dot are colored with brown. Another 4 clusters painted with purple, red, yellow, and green color have 2, 3, 4, and 5 Ag dots respectively. The biggest cluster has 11 dots colored with blue, and connects the top and bottom edges of the ZnO film. In the case of blue cluster, it is called percolating cluster, because the cluster percolates through the system. When the percolating cluster firstly appears, the occupation probability of sputtered Ag is denoted as percolation threshold, p_c [41-42].

The percolating cluster occurrence is directly associated with the coverage of the deposited film, which is in turn dictated by the thickness of deposited film. In the case of Ag/ZnO system, as the thickness of Ag film is increasing, the film becomes continuous gradually, and at certain thickness, there will be an Ag cluster appeared, which percolates the ZnO film either from the top to bottom, or from the left side to right side. When the percolation happens, the electrons in the Ag islands do not need to overcome huge ZnO barrier to conduct current. Instead, they can pass through the percolating cluster to transfer current from one side of the film to the opposite side freely, which dramatically decreases the resistivity of the whole film.

3.2.e Metallic Zone

After the first Ag percolating cluster appears and the Ag film keeps growing, the Ag film becomes continuous gradually and there are more percolating Ag clusters appeared on the ZnO film. Due to the fact that the numbers of free electrons increase tremendously and there are much more carriers in the system, the whole film begins to exhibit the metallic materials characteristics, so the Ag/ZnO system at this stage is categorized as metallic zone.

However, the electrical characteristics of the Ag thin film are significantly different from bulk Ag due to the size effect. The electron mean free path (EMFP), a term that indicates the average distance of two subsequent collisions, is used to characterize the resistivity of materials. In bulk metal, the resistivity is mainly

caused by the collisions between the conducting electrons and the impurities, defects, and lattices. When the thickness of metal film is decreased to several nanometers, which is much less than the EMFP of corresponding bulk one, the probability for electrons to collide with the interfaces becomes much higher than that of defects or impurities, so the size effect of the thin film becomes the dominant factor to determine resistivity of the system.

Firstly, the conductivity of bulk metal is given by [24-25]

$$\sigma_0 = \frac{ne^2}{m}\tau = \frac{ne^2}{m}\frac{\lambda_0}{v} \quad (24)$$

Where n=the number of electrons per unit volume

e=The charge of an electron

λ_0=The mean free path of electrons in bulk metal

v=The velocity of the electrons at the surface of the Fermi distribution

τ=The relaxation time (which can be interpreted as the average time between two consecutive collisions)

m=The mass of electrons

In terms of the resistivity of thin metal film, the number of electrons per unit volume is given by [24-25]

$$n = N(v,z)dxdydzdv_x dv_y dv_z \quad (25)$$

Where N(v,z)=number of electrons that is in the function of velocity (v) and position (z)

dxdydz=unit volume

$dv_x dv_y dv_z$=derivatives of velocity in x, y, and z directions

The change of number of electrons is caused by the several reasons, such as the motion of the electrons, the scattering of electrons, and the acceleration of the electrons by the electric field. Take into account all the possible scattering conditions, so the number of electrons per unit volume is given by [24-25]

$$n(v,z) = \frac{eF\tau}{m}\frac{\partial N_0(v,z)}{\partial v_x}[1 + \varphi(v)\exp(-\frac{z}{\tau v_x})] \quad (26)$$

Where φ(v)=an arbitrary function of v

N_0=an ordinary Fermi distribution function

F=the electric field that accelerated the electrons in the thin film

v_x=the velocity at the x-direction

According to the boundary conditions, the n is obtained based on the sign of v_z,

If v_z>0,

$$n = \frac{eF\tau}{m}\frac{\partial N_0}{\partial v_x}[1 - \exp(-\frac{z}{\tau v_x})] \quad (27)$$

If v_z<0,

$$n = \frac{eF\tau}{m}\frac{\partial N_0}{\partial v_x}[1 - \exp(\frac{t-z}{\tau v_x})] \quad (28)$$

The current density J is given by

$$J = evn = e\int v_x n dv_x dv_y dv_z \quad (29)$$

The mean current density is obtained by averaging all values of z from 0 to 1.

Based on the equation 30,

$$J = \sigma\varepsilon \tag{30}$$

Where σ=The conductivity of the thin film

ε=The electric field

The general equation for the thin film resistivity is given by

$$\frac{\sigma}{\sigma_0} = 1 + \frac{3}{4}\left(k - \frac{k^3}{12}\right)B(k) - \frac{3}{8k}\left(1 - e^{-k}\right) - \left(\frac{5}{8} + \frac{k}{16} - \frac{k^2}{16}\right)e^{-k} \tag{31}$$

Where $k = \frac{t}{\lambda_0}$

t=the thickness of the thin film

λ_0=the mean free path of electron in silver

$$B(x) = -Ei(-x) = \int_x^{\infty} \frac{e^{-t}}{t} dt$$

All the calculations above are derived based on the theory that all the electrons were reflected randomly from the film interfaces, meaning that all collisions at the interfaces are inelastic scattering. However, there is no way to tell whether the interface scattering is elastic or inelastic, so the proportion of elastic scattering is introduced, which is denoted as p'. When p' equals 0, it means that all the electrons in the films experience inelastic scattering at the interfaces. If p' equals 1, the collisions between the electrons and interfaces do not cost any energy, so the resistivity of the thin film is the same as corresponding bulk one. As p' increases from 0 to 1, there are more elastic scattering occurred in the thin film system, and the size effect becomes an unimportant factor increasingly.

When p’ is taken into account, Fuchs [24] and Sondheimer [25] come up with a general equation of the thin film resistivity given by

$$\rho = \rho_0[1 - \frac{3(1-p')}{2k}\int_1^{\infty}(\frac{1}{t^3} - \frac{1}{t^5})\frac{1-e^{-kt}}{1-pe^{-kt}}dt]^{-1} \quad (32)$$

Where ρ_0=The resistivity of bulk metal

$k = \frac{t}{\lambda_0}$

t=The thickness of the thin film

λ_0=The electron mean free path of electron in bulk material

When the thickness (t) of the metal film is very thin, which is much smaller than the EMFP of bulk metal (λ_0), the thin film resistivity can be approximated to

$$\rho = \rho_0 \frac{4}{3}\frac{1-p'}{1+p'}\frac{1}{klog(1/k)} \quad (33)$$

3.3 Simulation Procedure

Mathematica [43] was used to simulate the conduction mechanism of tunneling and thermionic emission with the evolution of Ag islands morphology in the dielectric regime. In order to simplify the simulation, but still obtain accurate results, several important parameters were approximated in a reasonable range, which were the average radius of Ag islands (r), the Ag coverage on the ZnO film (p), and the applied voltage (V). Since in the dielectric regime, the average radius was relatively small compared to the separation between the Ag islands; also, the radius only played a role in the activation energy. Thus, r is estimated as 10nm, which is also a reasonable number confirmed by the SEM

images (shown in Fig 4.1). In terms of the Ag area coverage (p), it only played a role in the activation energy calculation as well, so 50% is a reasonable value. Lastly, the applied voltage (V) is the potential drop across the gap over two neighboring Ag islands, which is difficult to estimate, because it depends on the experimental conditions. According to the experimental setup and the actual simulation work, 10^{-4} V potential drop across a couple of nanometers separation is a reasonable estimation. The equations used for the conduction mechanism simulation were equation 9 and 22 with islands separation ranging from 2 nm to 14 nm.

The simulation for the continuous Ag film was also used Mathematica [43]. Three p's were taken into account for the simulation of resistivity of Ag thin film, which were 0, 0.5, and 1. The equation used for the simulation was equation 33 with the Ag thickness ranging from 2 nm to 15 nm, and the bulk resistivity of Ag is 1.59×10^{-6} Ωcm [44].

3.4 Simulation Results

The simulation focused on dielectric zone and metallic zone. In the dielectric regime, the current density and resistivity were simulated with respect to the evolution of the separation between the neighboring Ag islands. In the metallic zone, since the Ag film has become continuous, the resistivity is simulated in terms of the Ag film thickness.

3.4.a Simulation of Conduction Mechanism in Dielectric Zone

Based on the equation 9, it describes the current density of thermionic emission, and the simulation result is shown in Fig. 3.9.

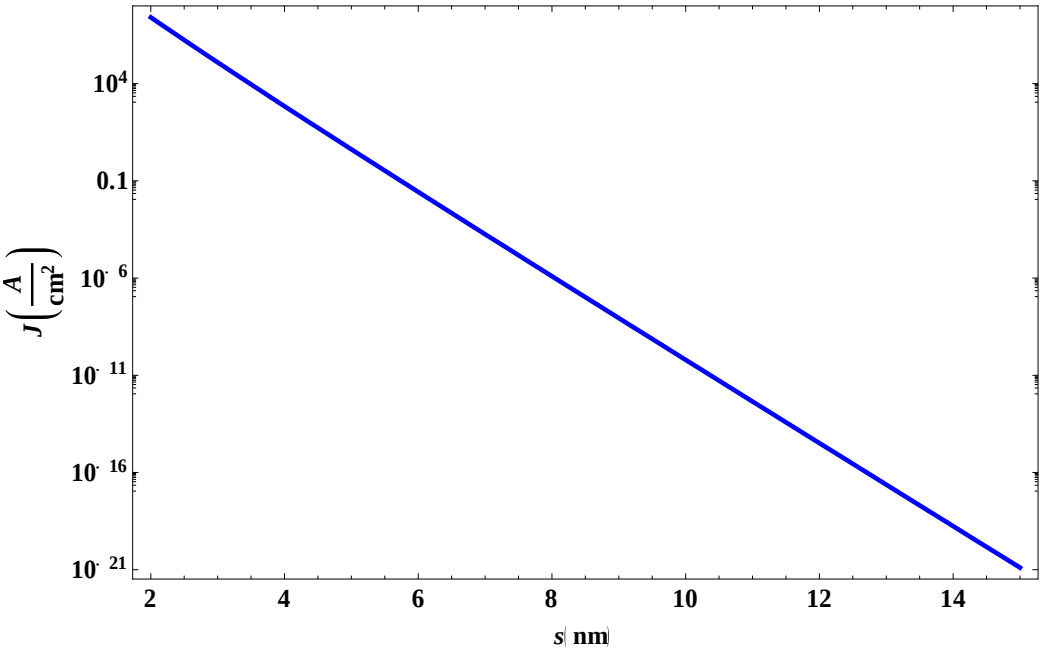

Fig. 3.9 The simulation of activated tunneling current density vs. the separation between two neighboring Ag islands

Based on equation 22, it describes that current density of activated tunneling, and the simulation result is shown in Fig. 3.10.

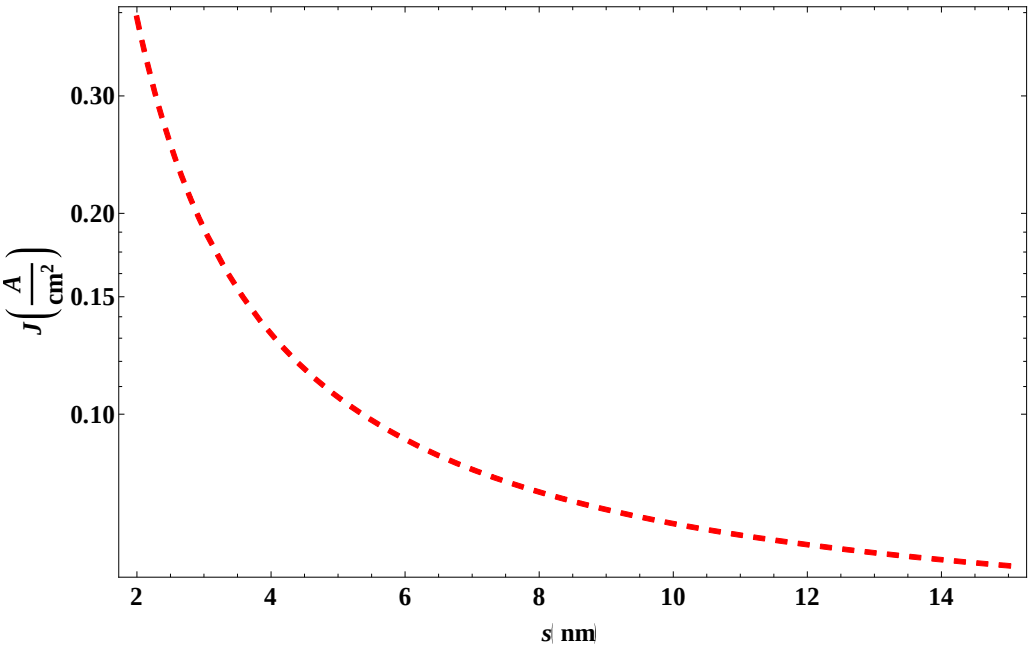

Fig. 3.10 The simulation of thermionic emission current density vs. separation between two neighboring Ag islands

The simulation figures of thermionic emission and activated tunneling were overlaid in the same figure shown in Fig. 3.11. Since the bigger current density would dominate the conduction corresponding to each separation (s), the total trend was marked as light black in Fig.3.11.

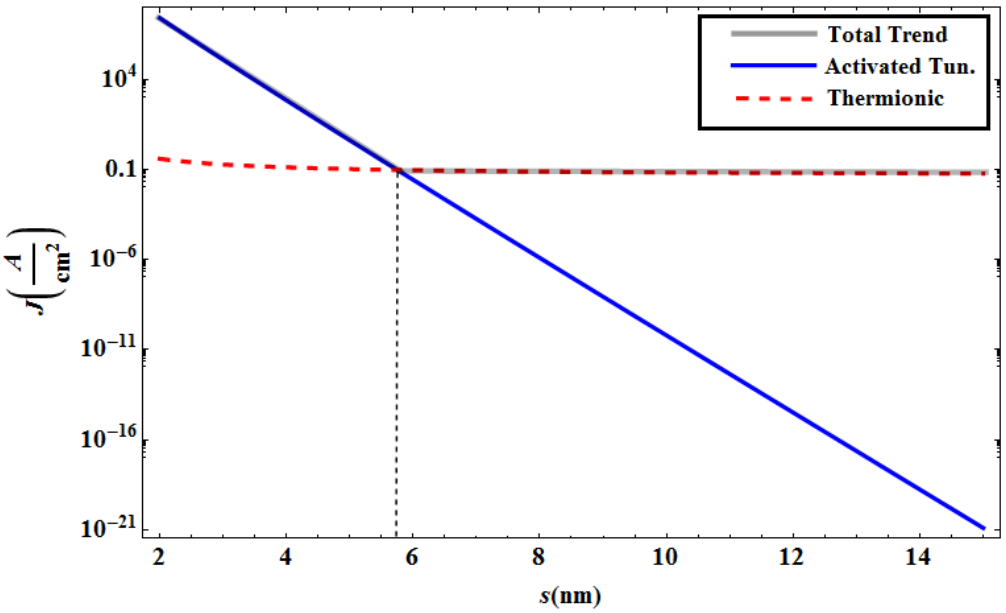

Fig. 3.11 The overlay of Fig. 3.9 and 3.10, the activated tunneling is colored with blue, and the thermionic emission is in red. The total trend is marked as grey line

Due to the relation between the current density and resistivity given by

$$\rho = \frac{V}{Js} \tag{34}$$

Where ρ=The effective resistivity of the thin film

V=Applied voltage across the ZnO separation

s=The separation between two neighboring islands

J=The current density

Therefore, the effective resistivity of the thermionic emission and activated tunneling is shown in Fig. 3.12.

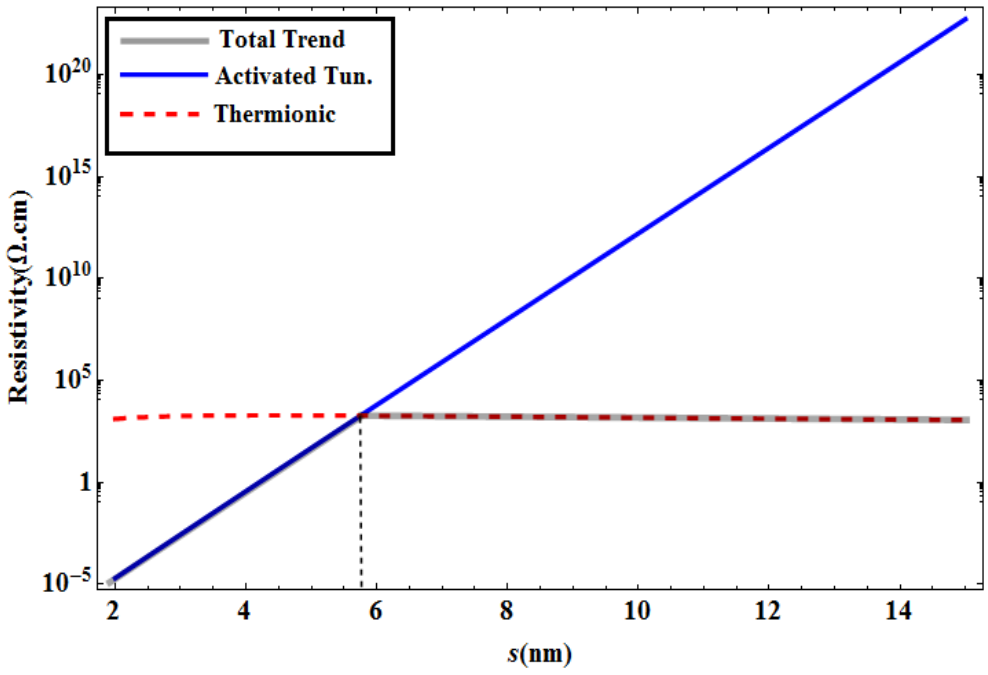

Fig. 3.12 The resistivity of thermionic emission and activated tunneling vs. the separation between two neighboring Ag islands

3.4.b Simulation of Conduction in Metallic Zone

According to the equation 32, when p' equals to 1, meaning that there is no inelastic scattering at the interfaces, the resistivity of thin Ag film turned out to be that of the bulk Ag. If the probability of elastic interface scattering equals to 0.5 and 0 respectively, the resistivity is shown in Fig. 3.13.

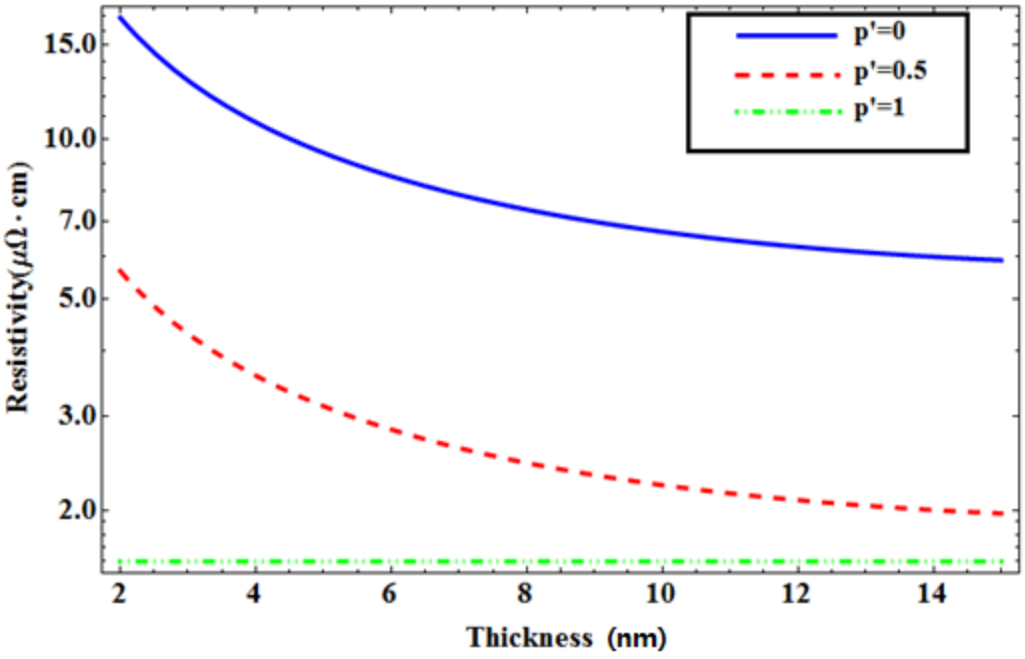

Fig. 3.13 The simulation of resistivity of Ag thin film vs. the thickness of the Ag film when p'=0, 0.5, and 1.

3.5 Discussion

In the dielectric zone, the Ag thickness was very thin, so the coverage of Ag was small and some discrete Ag islands were formed on ZnO film. As the Ag thickness was increased, it was estimated that the islands size would increase and the separation would decrease. However, since islands size only played little role in the simulation, the average radius of Ag islands was set up as a constant value. Therefore, the evolution of Ag film in the dielectric regime can be considered as two Ag islands with constant size moving towards each other shown in Fig. 3.14.

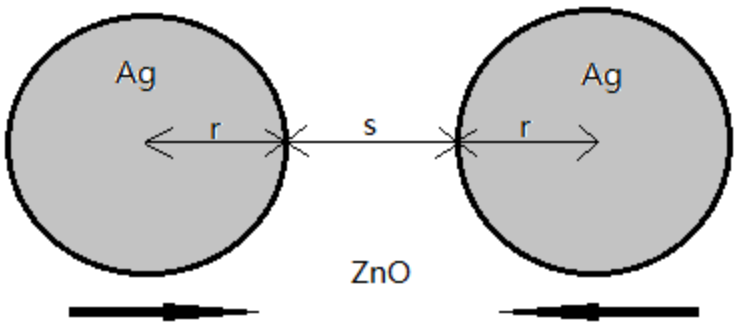

Fig. 3.14 The simplified evolution of Ag morphology on the ZnO film in the dielectric zone

Based on the simulation shown in Fig. 3.12, as the two Ag islands were moving towards each other from 14 nm away, the thermionic emission had much bigger current density, thus the effective resistivity was smaller initially. Due to the fact that electrons would choose less resistive path during transport, the thermionic emission conduction mechanism dominated in Ag/ZnO thin film system. When their distance was decreased to 6 nm, the current density of activated tunneling began to increase sharply and was close to that of thermionic emission. Once the distance was smaller than 6 nm, the current density of activated tunneling became larger than that of thermionic emission. Therefore, the activated tunneling conduction mechanism began to dominate the system. As the separation kept decreasing, the resistivity resulting from the tunneling mechanism reduced dramatically. When the separation between two Ag islands was only 2 nm, the effective resistivity was decreased to about 10^{-5} Ωcm.

Based on the analysis above, the Ag/ZnO thin film resistivity can be considered as resistivity resulting from the thermionic emission and activated tunneling paralleled together, so corresponding to each separation, the conduction mechanism that exhibited lower resistivity would dominate the system. The conduction model of the Ag/ZnO film was shown in Fig. 3.15.

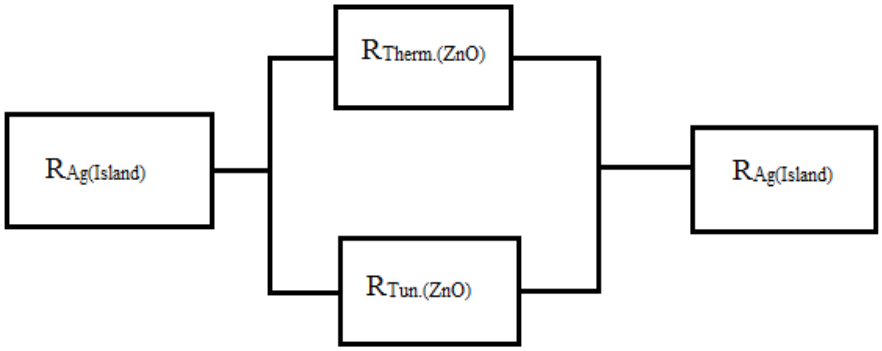

Fig. 3.15 The resistance series of Ag/ZnO film in the dielectric zone

In terms of the Ag thin film resistivity, as shown in Fig. 3.13, when p' equaled to 1, the resistivity of the Ag thin film was the same as that of bulk Ag, because the collision occurred at the interface did not cost energy, indicating that the size effect did not play a role in this case. As p' was decreased, meaning that the probability of inelastic scattering occurrence was increasing, the interface scattering became a dominant factor gradually and the resistivity of the Ag thin film increased. Considering the effect of the Ag thickness, as long as p' did not equal to 1, as the Ag thickness decreased, the resistivity increased greatly, because the EMFP in the thin film was determined by the thickness of the thin

film. When the Ag was becoming thinner, there would be more collision occurred at the interfaces, which in turn increased the resistivity.

3.6 Conclusion

In the dielectric zone, two conduction mechanisms were considered, which were thermionic emission and activated tunneling. Based on the simulation of current density and resistivity of the Ag/ZnO thin film system with respect to the islands separation (s), it was shown that when the "s" was beyond 6 nm at room temperature, the thermionic emission dominated the thin film system; once "s" was less than 6 nm, activated tunneling became the dominating conduction mechanism. Therefore, the transition "s" of thermionic emission and activated tunneling was 6 nm in the Ag/ZnO thin film system. As the thickness of the Ag was increased, there would be one or several percolating Ag clusters appeared, and the resistivity of the system could dramatically drop simultaneously. This region was called percolation zone. When the Ag film kept growing, it was expected that the metal film would become continuous gradually and exhibit the characteristics of metallic materials, which was classified as metallic zone. In this stage, the simulation of Ag thin film resistivity in terms of Ag thickness was carried out. Based on the simulation, it was seen that as the thickness increased, the resistivity of the Ag film reduced, and then approached to the resistivity of bulk Ag due to the increase of EMFP determined by the Ag thickness.

Chapter 4

THE EFFECT OF SILVER THICKNESS ON THE ELECTRICAL PROPERTIES OF Ag/ZnO WITH RESPECT TO THE Ag MIRCOSTRCTURE

4.1 Introduction

Since TCOs have the advantages of low resistivity and high transmittance, they are widely used as transparent electrodes in the optoelectronic devices, such as LCD, OLED, and photovoltaic solar cells [5]. The most used TCOs in the industry are indium tin oxide (ITO) [5]. ITO exhibits the metallic electrical characteristics (resistivity is about 10^{-4} Ωcm) and high transmittance as high as 90% [7-8], but the major disadvantage is the high cost. In order to find out cost effective TCOs to replace ITO, a lot of methods have been studied. Among them, TCO/Metal/TCO (TMT) structure has received a lot of attentions recently as a prospective ITO substitute. The strengths of this method are easy to operate and low cost, since only sputtering technique is required.

Although the TMT structure has yielded a desirable figure of merit (FOM), the overall performance is still not as good as ITO or doped TCOs [5-6, 12-13]. In order to further tailor the electrical and optical properties of the TMT structure, the more detailed investigation of the function mechanism is needed, and it is anticipated that the metal microstructure would be the key to the thin film system performance. Attempting to acquire a better view of the inserted metal

microstructure, in this work the top TCO layer is removed, so the metal morphology can easily be observed by using SEM.

Flexible substrate has become a very popular topic, because it has a lot of advantages compared to glass substrate, such as light weight, difficult to break, and space-saving. Therefore, both flexible substrate polyethylene napthalate (PEN) and glass were used as the thin films substrates.

In this work, the evolution of the Ag morphology is observed by using SEM, which exposes the Ag topographical characteristics in dielectric zone, percolation zone, and metallic zone. In order to relate the Ag morphology to the thin films electrical properties, Hall measurement and four point probe measurement are performed at different Ag thickness. It turns out that the measured resistivity and sheet resistance fit resistivity simulation well, which supports the proposed conduction models.

4.2 Experimental

Ag/ZnO thin films were deposited by using DC and RF sputtering techniques respectively. The thin film systems were prepared on flexible (PEN) and rigid (glass) substrate, and ZnO and Ag metal sputter targets were used for sputtering. Before the sputtering was carried out, the base pressure was approximately $1x10^{-7}$ Torr. During the deposition process, the pressure in the chamber was about 10 mTorr in pure argon atmosphere. The thickness of the ZnO

thin film layer was 30 nm, and the top Ag thickness varied from 2 nm to 10 nm in steps of 2 nm.

The thickness of the ZnO and Ag layer was verified by the Rutherford backscattering spectrometry (RBS) with a General Ionex Tandetron accelerator. The imaging was carried out under the pressure of $1x10^{-7}$ Torr. The energy of the incident He ion beam was 2.0 MeV and the total accumulated charge was 10 μC. In order to place the backscatter detector directly below the incident beam, samples and detector were in the Cornell geometry. The samples were tilted 55° off the normal incidence and at a scattering angle of 170°. Energy spectra were obtained using a surface-barrier detector and were analyzed with the aid of the RUMP computer-simulation program [45]. The Ag morphology was evaluated by using Philips XL 300 scanning electron microscopy (SEM). The SEM samples were cut into a square shape about 8x8 mm^2.

The effective resistivity of the samples was measured by the Hall measurement and the sheet resistance measurement was carried out by using four point probe setup. ImageJ [46] software was used to determine the morphological information of the Ag film, such as the average islands size, the separation between neighboring Ag islands, and the Ag coverage.

4.3 Results

RBS was used to evaluate the Ag thickness. Since every 8 seconds sputtering under the experimental conditions increased the Ag thickness approximately by 2 nm, the Ag thickness were grown for 8, 16, 24, 32, and 40 seconds, which corresponded to 2, 4, 6, 8, and 10 nm Ag thickness respectively.

The SEM images of the Ag morphology evolution with the increase of the Ag thickness were shown in Fig. 4.1.

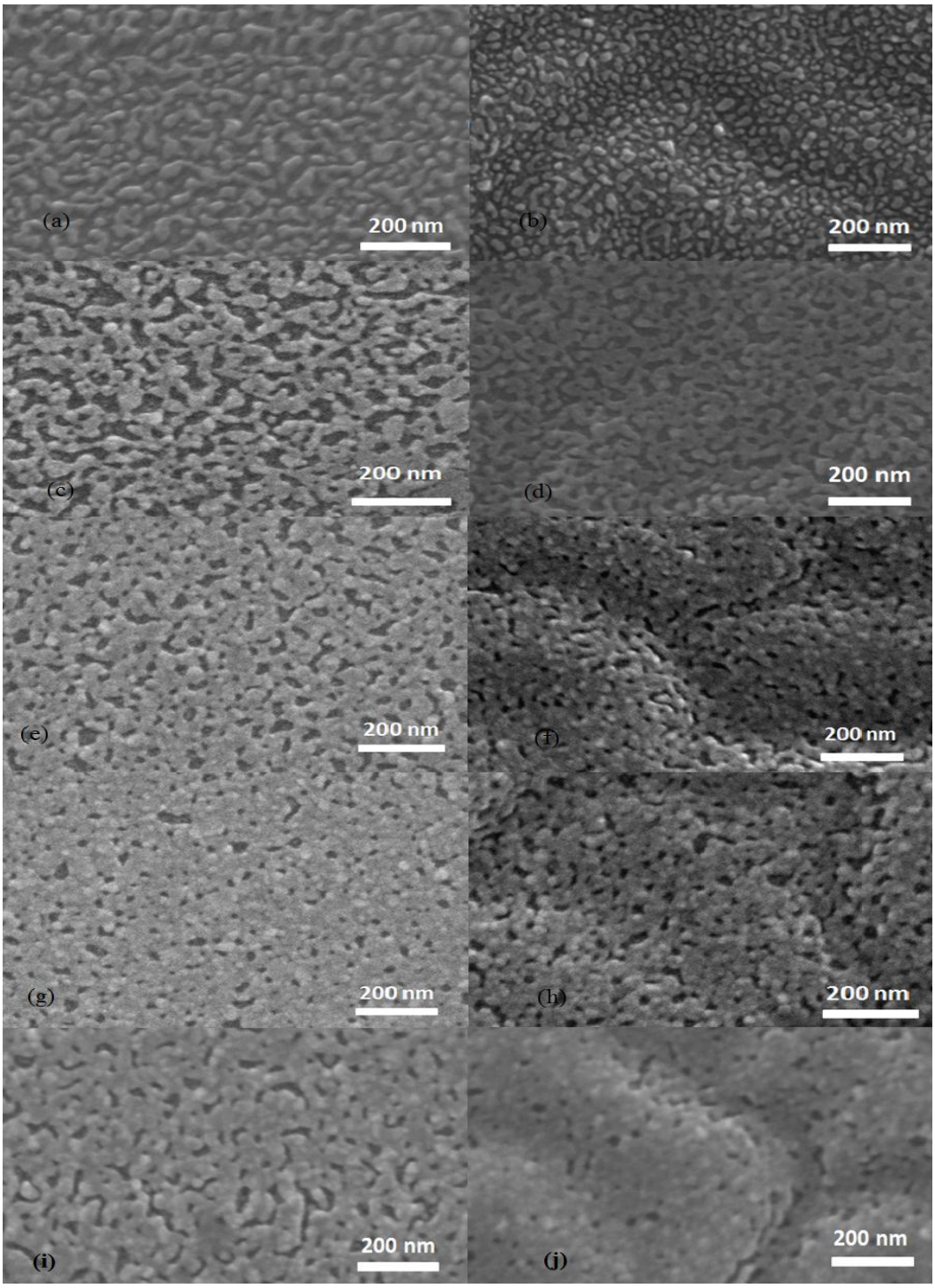

Fig. 4.1 (a) and (b) for 2 nm Ag/ZnO on Glass and PEN substrate respectively; (c) and (d) for 4 nm Ag/ZnO on Glass and PEN substrate respectively; (e) and (f) for 6 nm Ag/ZnO on Glass and PEN substrate respectively; (g) and (f) 8 nm Ag/ZnO on Glass and PEN substrate respectively; (i) and (j) 10 nm Ag/ZnO on Glass and PEN substrate respectively.

By using ImageJ software, the distribution of the islands size (r) and inter-islands spacing (s) were evaluated. In order to determine the “s” and “r”, a metallurgical method called linear intercept method, which was usually used to evaluate the grain size, was introduced [47] in this work. In the case of 2 nm Ag/ZnO system, due to the fact that the Ag islands were discontinuous, “r”, which was designated as the radius of the spherical shape islands in the simulation, here signified one half of the islands size measured by the linear intercept technique. “s” still meant the gap between two neighboring Ag islands. When the Ag film passed the percolation threshold, the film became continuous. In this case, “s” indicated the size of the voids, where the ZnO had not been covered by Ag. “r” in this case cannot refer to the islands size, because there were no individually islands on the ZnO film. However, attempting to show the evolution of the Ag film, it meant that the separation between voids. The distributions of the r and s were shown in Fig. 4.2.

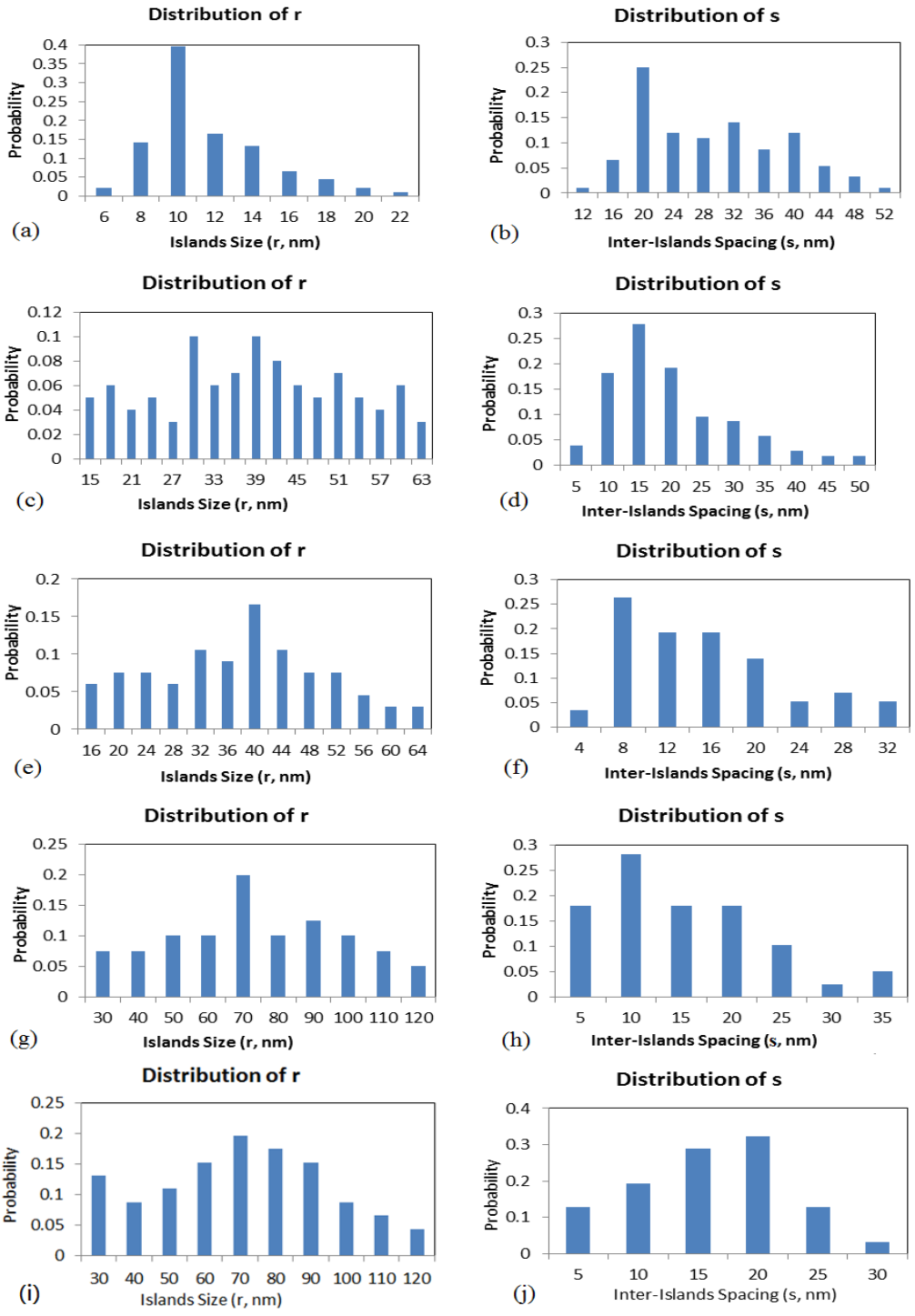

Fig. 4.2 (a) and (b) shown the distribution of r and s with 2nm Ag/ZnO; (c) and (d) shown the distribution of r and s with 4 nm Ag/ZnO; (e) and (f) shown the distribution of r and s with 6 nm Ag/ZnO; (g) and (h) shown the distribution of r and s with 8 nm Ag/ZnO; (i) and (j) shown the distribution of r and s with 10 nm Ag/ZnO.

The average r, s and coverage of Ag were shown as follows,

	Average Islands Size (r, nm)	Average Inter-Islands Spacing (s, nm)	Ag coverage (%)
2 nm Ag/ZnO	13	32	50
4 nm Ag/ZnO	35	20	73
6 nm Ag/ZnO	41	17	85
8 nm Ag/ZnO	73	16	93
10 nm Ag/ZnO	71	16	92

Table 1 The average islands size (r), inter-islands spacing, and Ag coverage of 2/4/6/8/10 nm Ag/ZnO/Glass thin film systems

Plot the evolution of r, s and coverage in Fig. 4.3, 4.4, and 4.5.

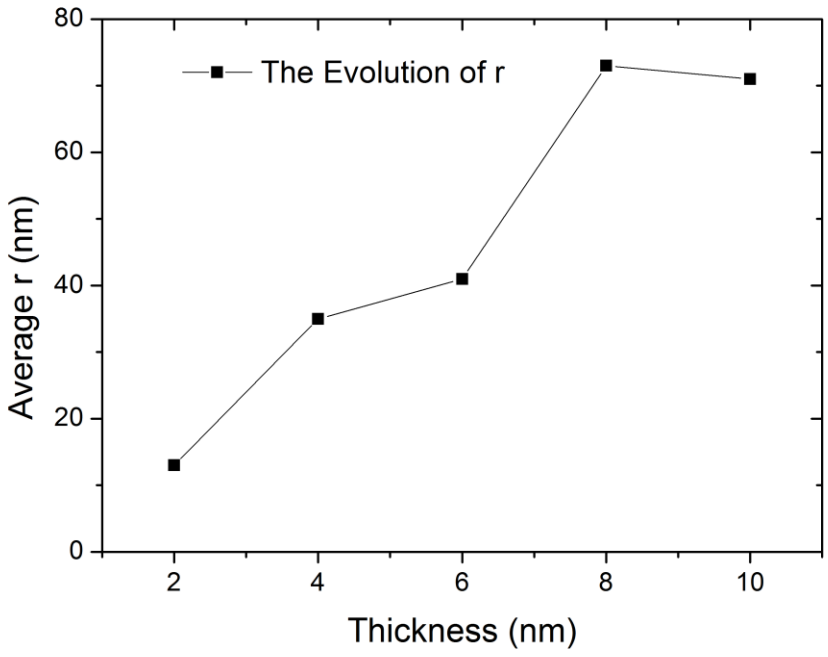

Fig. 4.3 The evolution of the average islands size (r) with respect to the Ag thickness varying from 2nm to 10nm

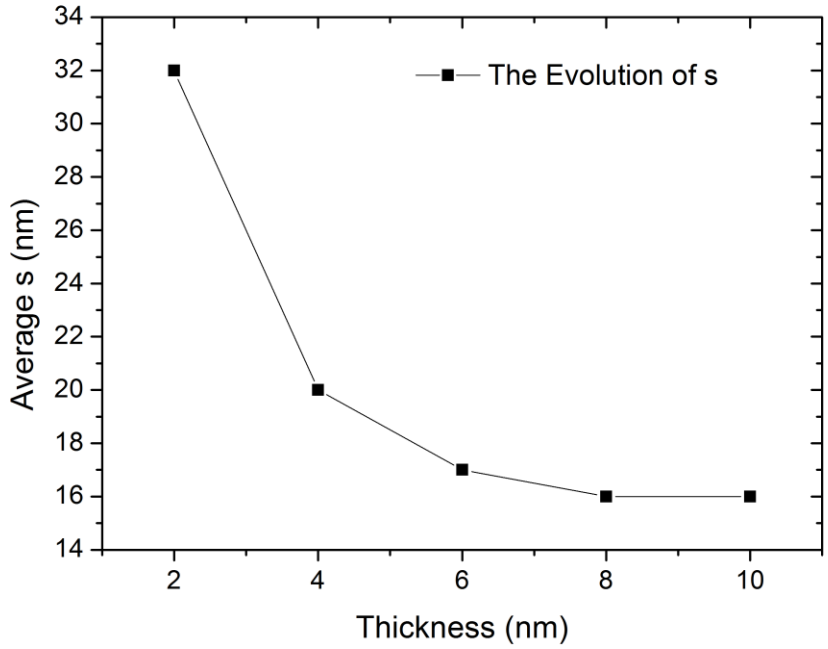

Fig. 4.4 The evolution of the average inter-islands spacing with respect to the Ag thickness varying from 2nm to 10nm

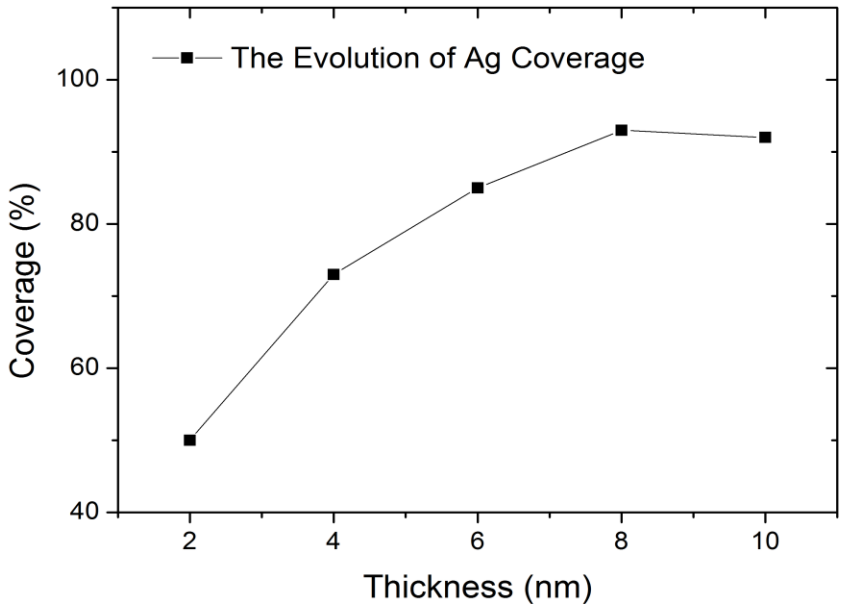

Fig. 4.5 The evolution of the Ag coverage with respect to the Ag thickness varying from 2nm to 10nm

In order to relate the Ag morphology to the electrical properties of the thin film systems, the effective resistivity and sheet resistance measurements were performed by using Hall measurement and four point probe measurement respectively. When Ag thickness was 2 nm, due to the extremely high resistivity, both measurements did not work, so the measurements of 2 nm Ag/ZnO system did not mention in this section, but this issue would be discussed in next section. The resistivity and sheet resistance of thin films with Ag thickness varying from 4 nm to 10 nm were reported. The electrical properties of Ag/ZnO thin films on PEN and glass were shown below,

	Resistivity (Ωcm)	Sheet Resistance (Ω/Square)
4nm Ag/ZnO/PEN	7.21×10^{-4}	206
6nm Ag/ZnO/PEN	5.41×10^{-4}	64
8nm Ag/ZnO/PEN	1.32×10^{-4}	58
10nm Ag/ZnO/PEN	1.15×10^{-4}	19

Table 2 The resistivity and sheet resistance of the 4/6/8/10 nm Ag/ZnO thin films on PEN substrate

	Resistivity (Ωcm)	Sheet Resistance (Ω/Square)
4nm Ag/ZnO/Glass	2.88×10^{-4}	92
6nm Ag/ZnO/Glass	1.12×10^{-4}	19
8nm Ag/ZnO/Glass	1.01×10^{-4}	10
10nm Ag/ZnO/Glass	9.29×10^{-5}	10

Table 3 The resistivity and sheet resistance of 4/6/8/10 nm Ag/ZnO thin films on glass substrate

Plot the resistivity and sheet resistance of the Ag/ZnO system on PEN and glass substrate in Fig. 4.6 and 4.7.

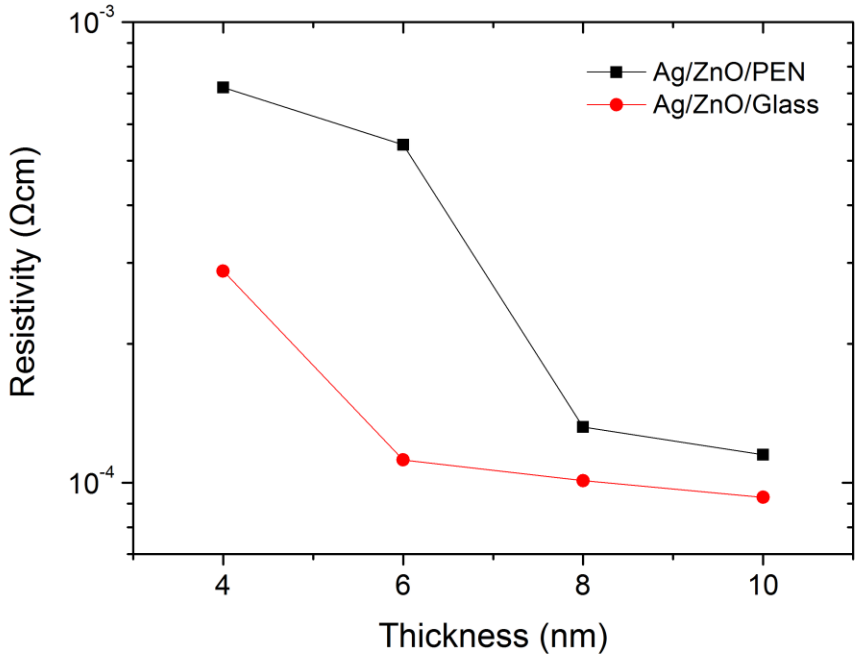

Fig. 4.6 The resistivity vs. Ag thickness on PEN and glass substrate

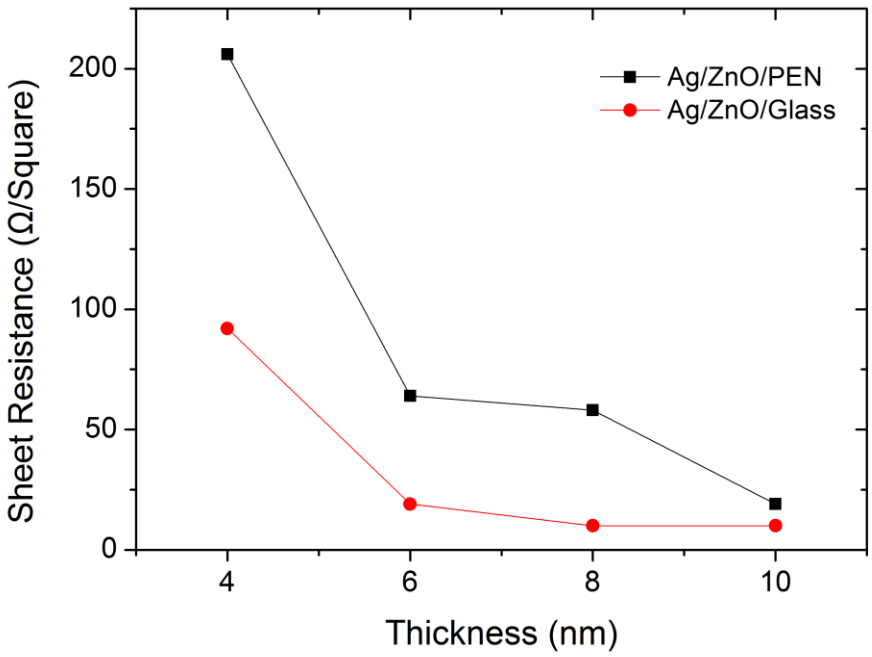

Fig. 4.7 The sheet resistance vs. Ag thickness on PEN and glass substrate

4.4 Discussion

Based on the SEM images, when the Ag was 2 nm thick, discontinuous Ag islands were formed on the ZnO surface. The average islands size at this stage was 13 nm, and the spacing between Ag islands was approximately 32 nm, which was relatively a large value. In terms of the distribution of the “r” and “s”, it was shown that both of them had wide distributions, which indicated that the sputtered Ag islands were in very irregular shape other than spherical shape as expected in the simulation. Therefore, it was estimated that when “s” was still relatively large, the irregular shape Ag islands would have the strong tendency to interconnect

with each other and form Ag clusters. Therefore, the percolation threshold would be smaller than it was anticipated when Ag islands were in regular shape.

As talked above, the effective resistivity and sheet resistance in this stage was too large to measure. According to the specifications of the Ecopia HMS-3000 Hall Effect Measurement System, the upper resistivity limit of the setup is 10^7 Ωcm, so the resistivity of the 2 nm Ag/ZnO system should be close to this value. Since the average "s" equaled to 32 nm, based on the simulation shown in Fig. 3.12, the dominating conduction mechanism was thermionic emission. After the "r" and "s" were substituted in the equation 9 and 34, the effective resistivity was calculated as 6.1×10^6 Ωcm, which was a reasonable result. Therefore, the actual Ag morphology and the measurements supported the simulation model in the dielectric zone. Based on this result, a series conduction model was proposed shown in Fig. 4.8.

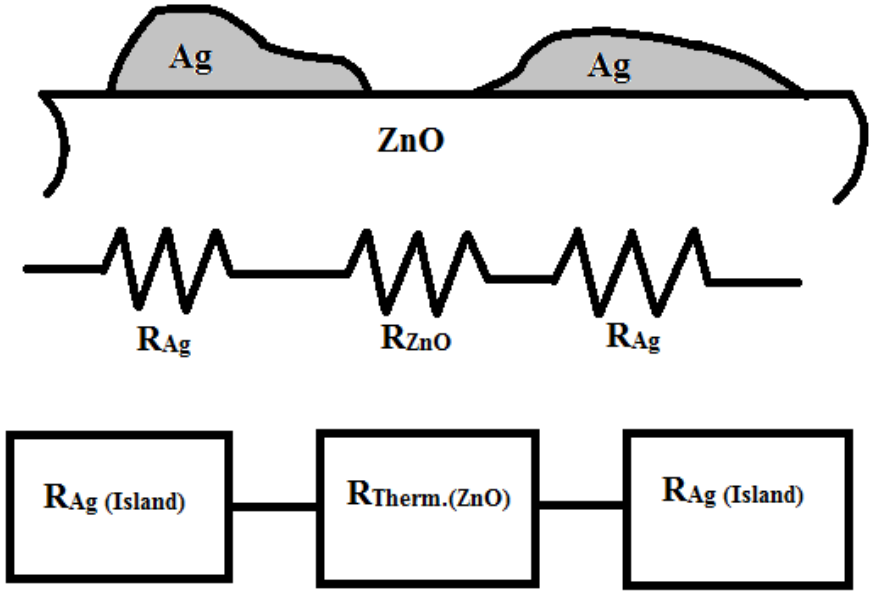

Fig. 4.8 The Ag thin film morphology and series resistance model in the dielectric zone

The SEM images exposed that as the thickness of Ag increased, the Ag film became continuous gradually. When the Ag thickness was 4 nm, it was shown that the discrete Ag islands began to coalesce and a lot of Ag clusters were appeared. According to the percolation theory, the percolating cluster indicates the cluster that connects the opposite edges of the system. As marked in the Fig. 4.9. There were some clusters already percolated the ZnO film. Although the average “s” was still large, about 20 nm, due to the wide distribution of “r” and “s”, the discrete Ag islands had already coalesced and a lot of Ag clusters were formed. Some of the clusters had percolated the system. Therefore, the percolation threshold was estimated between 0.5 (the Ag coverage in 2 nm

Ag/ZnO system) and 0.73 (the Ag coverage in 4 nm Ag/ZnO system). In order to determine the exact percolation threshold in Ag/ZnO system, more SEM images with respect to more specific Ag thickness ranging from 2 nm to 4 nm were needed, 0.6 was a reasonable estimation of the percolation threshold of Ag/ZnO thin films in these experimental conditions.

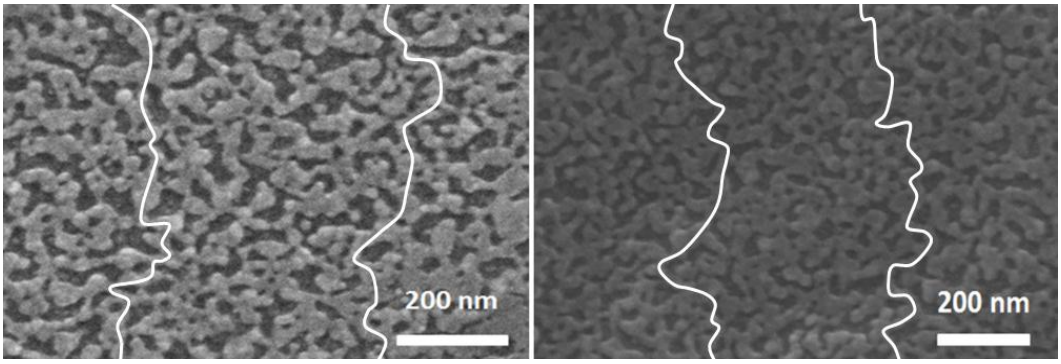

Fig. 4.9 The percolating clusters were marked in the 4nm Ag/ZnO thin film system

After the Hall measurement and four point probe measurement were performed, the effective resistivity of the 4nm Ag/ZnO system on PEN and glass substrate both exhibited a tremendous drop, which was 7.21×10^{-4} Ωcm and 2.88×10^{-4} Ωcm respectively. Thus, the experimental data proved the percolation theory in terms of the electrical characteristics of the thin films.

As the Ag thickness kept growing, the Ag film became more continuous, and no individual Ag islands were left. Thus, it was improper to refer "s" as the separation between Ag islands and "r" as the islands size. However, in an attempt to show the evolution of Ag film morphology, "s" and "r" were still used. "s" in

this regime indicated the size of voids, where the ZnO had not been covered by the Ag, and “r” referred to the separation between neighboring voids. As shown in the Table 1, the “s” was reduced to 17 nm, 16 nm and 16 nm with 6 nm, 8 nm, and 10 nm thick Ag respectively. Overall, as the Ag thickness increased, s was reduced, and when Ag film became continuous, “s” decreased slowly and approached to a “saturation” point, which was approximately 16 nm. “r” exhibited sharp increase from 13 nm to 73 nm first with Ag thickness increased from 2 nm to 8 nm. However, it was seen in the Fig. 4.3 and 4.5, when the Ag thickness was 10 nm, “r” did not increase, but surprisingly decreased by 2 nm; also, the Ag coverage was smaller than that of 8 nm Ag. It was probably because during the sputtering process, the temperature in the chamber would be relatively high due to the bombardment mechanism between Ag target and high energy incident ion beam, so sputtering at the same time had the characteristics of an annealing process. Therefore, the voids, where had not been covered by Ag, had the tendency to coalesce and merge [48], which could explain the trend of “r” and coverage. However, the thin film growth would still be the dominating trend, so “s” was expected to decrease slowly; yet, the coverage and “r” was anticipated to increase slowly and coverage would approach to 100% eventually.

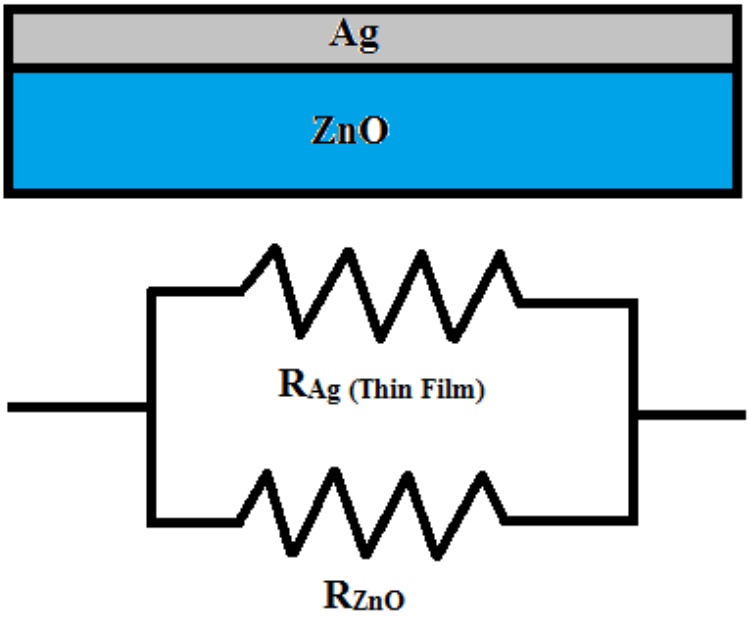

Fig. 4.10 The parallel resistance of Ag/ZnO thin film system when the Ag thickness was beyond the percolation threshold

In terms of the electrical properties of Ag/ZnO thin films in the metallic regime, in Fig. 4.6 and 4.7 it was shown that the effective resistivity decreased gradually, which satisfied the simulation shown in Fig. 3.13. Thus, when the Ag film became continuous, the overall resistance of the Ag/ZnO thin film system can be regarded as two layers paralleled each other shown in Fig. 4.10, and the layer that had lower resistivity dominated the conduction mechanism. Since Ag thin layer had much lower resistivity than ZnO layer, the Ag thin film determined the electrical properties of the whole system in the metallic zone.

However, compared the experimental data to the simulation results, it turned out that the experimental resistivity was one order bigger than simulated one, but it was still in the acceptable range due the following reasons. Firstly, the

simulation of Ag thin film resistivity with respect to Ag thickness assumed that the Ag film is a continuous layer, no matter how thin it was. However, in fact as shown in the SEM images, the film was not completely continuous, even though the Ag coverage was beyond 90%. Therefore, during the conducting electrons transport, they would encounter more collisions than anticipated in the simulation, which could be the reason that experimental resistivity was higher than the simulated one. Secondly, because the simulation showed the resistivity of pure Ag thin film, in fact since the Ag film was only several nanometers thick and dispersed on the ZnO film, it could be oxidized by the air, which increased the measured resistivity of the Ag film. Lastly, even though the Hall measurement was accurate, it was inevitable to have some errors, which could count for the discrepancy.

4.5 Conclusion

Based on the SEM images, the experimental data confirmed the simulations shown in the previous chapter. In the dielectric zone, based on the simulation model, the calculated effective resistivity was in the reasonable range. With 4 nm thick Ag, the SEM images showed that there were a lot of percolating clusters that had already appeared, so it was estimated that the effective resistivity would show a sudden drop, and experimental data proved the expectation. As the Ag thickness increased, the Ag film became continuous gradually and the effective resistivity exhibited a gradual decrease, which confirmed the simulation results of the Ag thin film resistivity.

Chapter 5

Conclusions

5.1 Summary

Based on the simulations and experiments, they clearly exposed the evolution of conduction mechanism of the Ag/ZnO thin film system with respect to the Ag morphology and thickness. In the dielectric zone, as the Ag thickness was extremely thin and the separation between Ag islands was very large, which was beyond the transition separation, 6 nm, the dominating conduction mechanism was thermionic emission; with Ag thickness below 6 nm, the major mechanism transited to activated tunneling. Since the Ag islands size exhibited wide distribution, indicating that their shapes were very irregular, they were likely to coalesce and form clusters. With 4 nm thick Ag, there were some percolating clusters formed in the system, and the effective resistivity of the system presented a tremendous drop, which supported the percolation theory. As Ag thickness was grown, the Ag film became continuous, and yet there were no individual islands or clusters left on the surface. The resistivity exhibited a gradual decrease as the Ag thickness increased. The reason was that the EMFP in thin film system was not determined by collisions between conducting electrons and defects or impurities, but by the boundary scattering, so the Ag thickness determined the EMFP. As Ag thickness increased, the EMFP was also increased. When the Ag thickness was close to the EMFP of bulk Ag, the effective resistivity of the thin Ag film also approached to the bulk Ag. The simulation and experimental data presented the same trend.

5.2 Future Work

Since the conduction mechanism of Ag/ZnO thin film system with respect to the Ag morphology has been fully understood, in order to yield higher FOM, efforts should be put into how to tailor the Ag morphology. As it was shown in this work, the Ag morphology determines the electrical property of the thin film system. If the morphology can be controlled, the thin film properties can be tailored, which could dramatically increase the resistivity without depositing too much Ag. There are two prospective methods, which are controlling the Ag deposition process and the ZnO morphology.

REFERENCES

[1] L. I. Maissel and M. H. Francombe, An Introduction to Thin Films, NY (1973).

[2] I. Markov, Materials Chemistry and Physics, **49**, 93-104 (1997).

[3] C. Argile and G. E. Rhead, Surface Science Reports, **10**, 277-356 (1989).

[4] H. Wei and H. Eilers, Journal of Physics and Chemistry of Solids, **70**, pp. 459-465 (2009).

[5] A. Indluru and T. L. Alford, J. Appl. Phys. **105**, 123528 (2009).

[6] H. Han, N. D. Theodore, and T. L. Alford, J. Appl. Phys. **103**, 013708 (2008).

[7] C. Guillen and J. Herrero, J. Appl. Phys. **101**, 073514 (2007).

[8] A. El Hichou, A. Kachouane, J. L. Bubendorff, M. Addou, J. Ebothe, M. Troyon, and A. Bougrine, Thin Solid Films, **458**, 263 (2004).

[9] X. Bai, E. G. Wang, P. Gao, and Z. L. Wang, Nano Letters, **3 (8)**, pp. 1147-1150 (2003).

[10] V. Bhosle, J. T. Prater, F. Yang, D. Burk, S. R. Forrest, and J. Narayan, J. Appl. Phys. **102**, 023501 (2007).

[11] K. H. Kim, K. C. Park, and D. Y. Ma, J. Appl. Phys. **81**, 7764 (1997).

[12] K. Sivaramakrishnan and T. L. Alford, Appl. Phys. Lett. **96**, 201109 (2010).

[13] K. Sivaramakrishnan, N. D. Theodore, J. F. Moulder, and T. L. Alford, J. Appl. Phys. **106**, 063510 (2009).

[14] Y. Xia and N. J. Halas, MRS Bulletin, **30 (5)**, pp. 338-348 (2005).

[15] K. Seal, M.A. Nelson, Z.C. Ying, D.A. Genov, A.K. Sarychev, and V.M. Shalaev, Phys. Rev. **B 67**, 035318 (2003).

[16] N. T. Liang, C. Y. Lu, and S. Wang, Solid State Communication, **51 (6)**, pp. 385-388 (1984).

[17] E. H. Rhoderick, IEE Proc. **129 (1)**, pp. 1-14 (1982).

[18] C. R. Crowell, Solid State Electronics, **8 (4)**, pp. 395-399 (1965).

[19] C. A. Neugebauer and M. B. Webb, J. Appl. Phys. **33**, pp. 74-82 (1962).

[20] R. M. Hill, Proc. R. Soc. Lond. **A 309**, pp. 377-395 (1969).

[21] J. E. Morris, T. J. Coutts, Thin Solid Films, **47**, 3-65 (1977).

[22] B. Abeles, P. Sheng, M.D. Coutts, and Y. Arie, Adv. Phys. **24**, pp. 407–461 (1975).

[23] W. Zhang, S. H. Brongersma, O. Richard, B. Brijs, R. Palmans, L. Froyen, and K. Maex, Microelectronic Engineering, **76**, pp. 146-152 (2004).

[24] K. Fuchs, Proc. Cambridge Philos. Soc. **34**, 100 (1938).

[25] E. H. Sondheimer, Adv. Phys. **1** (1952).

[26] T. L. Alford, L. C, Feldman, and J. W. Mayer, Fundamentals of Nanoscale Film Analysis (2007)

[27] D. K. Schroder, Semiconductor Material and Device Characterization, NY (2006)

[28] K. Sivaramakrishnan and T. L. Alford, Appl. Phys. Lett. **96**, 201109 (2010).

[29] F. C. M. Van De Pol, F. R. Blom, and TH. J. A. Popma, Thin Solid Films, **204**, pp. 349-364 (1991).

[30] F. R. Blom, F. C. M. Van De Pol, G. Bauhuis, and TH. J. A. Popma, Thin Solid Films, **204**, pp. 365-376 (1991).

[31] D. J. Kang, J. S. Kim, S. W. Jeong, Y. Roh, S. H. Jeong, and J. H. Boo, Thin Solid Films, **475**, pp. 160-165 (2005).

[32] K. Ellmer, J. Phys. D: Appl. Phys. **34**, pp. 3097-3108 (2001).

[33] J. G. Simmons, J. Appl. Phys. **34 (6)**, 1793 (1963).

[34] J. G. Simmons, J. Appl. Phys. **35 (9)**, 2655 (1964).

[35] J. G. Simmons, J. Appl. Phys. **35 (8)**, 2472 (1964).

[36] Z. Fan and J. G. Lu, Zinc Oxide Nanostructure: Synthesis and Properties (2005).

[37] T. J. Coutts, Electrical Conduction in Thin Metal Film, NY (1974).

[38] C. J. Gorter, Physica, **17**, 788 (1951).

[39] E. Darmois, J. Phys. Radium, **17**, 210 (1956).

[40] P. Bieganski, E. Dobierzewska-Mozrzymas, E. Pieciul, and G. Szymczak, Vacuum, **74**, pp. 211-216 (2004).

[41] B. Berkowitz and R. P. Ewing, Surveys in Geophysics, **19**, pp. 23-72 (1998).

[42] K. Christensen, Percolation Theory (2002).

[43] Wolfram Research, Inc., Mathematica, Version 8.0, IL (2010).

[44] Lazar Miriam, Let's Review: Physics, The Physical Setting (2007).

[45] L. R. Doolittle and Nucl, Instrum. Methods Phys. Res. **B 9**, 344 (1985).

[46] M. D. Abramoff, P. J. Magalhaes, and S. J. Ram, Biophotonics International, **11 (7)**, pp. 36-42 (2004).

[47] J. H. Han and D. Y. Kim, Acta Materialia, **46 (6)**, pp. 2021-2028 (1998).

[48] K. Sieradzki, K. Bailey and T. L. Alford, Appl. Phys. Lett. **79**, 3401 (2001).